VALIDITY OF KOZENY-CARMAN EQUATION IN CONSTANT-PRESSURE CAKE FILTRATION

by

Siying Zhang

B.S., Tianjin University, 2014

Submitted to the Graduate Faculty of

Swanson School of Engineering in partial fulfillment

of the requirements for the degree of

Master of Science

University of Pittsburgh

2015

UNIVERSITY OF PITTSBURGH

SWANSON SCHOOL OF ENGINEERING

This thesis was presented

by

Siying Zhang

It was defended on

November 23, 2015

and approved by

George E. Klinzing, Ph.D., Professor, Department of Chemical and Petroleum Engineering

John A. Keith, Ph.D. Assistant Professor, Department of Chemical and Petroleum Engineering

Thesis Advisor: Joseph J. McCarthy, Ph.D., Professor, Department of Chemical and Petroleum Engineering

VALIDITY OF KOZENY-CARMAN EQUATION IN CONSTANT-PRESSURE CAKE FILTRATION

Siying Zhang, M.S.

University of Pittsburgh, 2015

Filtration in the separation of solid-liquid mixtures has been studied for 90 years. However, the lack of a generalized set of laws for filtration has increased the difficulty of incorporating equations from one model into another. This thesis is focused on determining the relationship between fluid properties and cake structure on the void distribution and ultimate pressure drop during a filtration process. By comparing experimental results to those predicted from the Kozeny-Carman model/equation, we assess the utility of this equation for application to systems that include poly-disperse particles at moderate fluid pressure. We find substantial agreement between model and experiment only for systems that result in well-ordered particle packing (i.e., those that have a tight distribution of void sizes). Dramatic disagreement is observed for particle beds that exhibit wide void size distributions. The cake structure is primarily influenced by the size ratio of the particles that compose the cake; specifically, particles with a size ratio in which $R_{s/l}$ is larger than 0.5 do not typically form an ordered pore structure. We propose a modified Kozeny-Carman equation, based on a bimodal void distribution, by introducing two factors: the fraction of expanded voids (κ) and the ratio of void sizes (β). Discrete Element Method (DEM) simulations of the packing of poly-disperse spheres are used to analyze the cake structure for different size ratios of binary mixtures. Based on the simulation results, void size distributions of

the simulated beds can be extracted by means of a radical Delaunay tessellation. The void structure is quantified in terms of probability density functions of pore and constriction sizes. By fitting the simulated void size distributions to a bimodal (two normal) distribution, the factors κ and β can be calculated based on different mean void sizes and probability density. The predicted flow dynamics from the modified equation with factors extracted from the simulation results are found to be much more similar to the experimental flow rates than those calculated using the unmodified Kozeny-Carman equation. Therefore, the modified equation is deemed reliable at predicting the flow behavior, provided that an approximate representation of the void size distribution is available.

TABLE OF CONTENTS

LIST OF TABLES

LIST OF FIGURES

PREFACE

I would like to thank my advisor, Dr. Joseph J. McCarthy for his guidance and support during my project. All the technical knowledge and research skills I learnt from him enrich me to be a better graduate student. The rigorous scientific approach and innovative thinking I gained while working with him would benefit me for a lifetime.

I would also like to thank all the members of my Master thesis committee, Dr. George E. Klinzing and Dr. John A. Keith for their insightful comments and advises in my thesis.

I would also like to thank my friends and colleagues who study and work with me in Pittsburgh, especially, Melissa Lash for her help in study particle packing and Megan Cala, Siying Liu for their help in simulations. I am also grateful to Michael McMahon and Nicole Salamacha for their help with my filtration experiments.

Finally, I would like to dedicate this work to my parents, Lan Zhang and Shufang Sun, for their support and sacrifice. I would like to thank my cousins and grandparents for encourage and assist me every time I feel bad during my life. I also acknowledge all my friends for their kind help, especially, my boyfriend Jingran Su for his support in my journey.

1.0 INTRODUCTION

Filtration is a process that separates one phase of material from another phase. Types of filtration can be classified by different types of filters (i.e., cake filtration, frame filtration and candle filters). This thesis is focused on fluid flow through a porous cake, which is widely applied in groundwater flow, oil transport in porous rock, the permeation of ink in paper, and other engineering applications [1]. In this thesis, cake filtration is used. It is a technique that creates a cake – a layer that is composed of solids – on the filter that is then used to separate (additional) solid(s) from the liquid [2]. A porous cake, and its interconnect voids are a heterogeneous system. The void space allows fluid to pass through [3]. Cake filtration processes can be divided into four categories [4]:

- Constant pressure filtration
- Constant flow filtration
- Non-constant filtration: variable pressure, variable flow
- Stepped pressure filtration

In constant pressure filtration, an external pressure is added across the filter. In constant flow filtration, a positive displacement pump is used to push the liquid through at a constant flow rate [5]. A non-constant filtration is a pressure filter fed by a pump. A stepped pressure filtration is a system where pressure is increased by increments.

1.1 COVENTIONAL THEORY

Studies on cake filtration have been reported for over ninety years. They changed from simple restricted results to more exact and relaxed results. The conventional theory (as shown in Table 1) was developed during the beginning of the last century by Ruth, Grace, Tiller, and Shirato [6]. That is the mainstay in design calculations, scale-up, and data interpretation of cake filtration systems [1]. This theory is based on assumptions that the particle velocity is negligible and the fluid flow follows Darcy's law. This indicates that the flow rate of fluid in the filtration process is directly proportional to the ultimate pressure drop and inversely proportional to the flow resistance between the cake and the medium [1]. Notation:

q_l	superficial liquid velocity	p_{s_m}	compressive stress at interface
k	cake permeability	R_m	medium resistance
μ	fluid visocosity	V	cumulative filtrate volume
p_l	liquid (filtrate) pressure	w	cake mass
x	distance away from medium	t	time
s	particle mass fraction	t_m	fictitious time
$\bar{m}$	wet to dry cake mass ratio	Q	constant filtration rate
P_0	operating pressure	α	specific cake resistance
P_a	quantity pressure	δ	exponent factor
ε_s	cake solidosity	β	exponent factor
ε_s^0	cake solidosity at the zero stress	L	cake thickness
α_{av}	average specific cake resistance		

Table 1. Main results of the conventional theory of cake filtration [1]

Basic equations	
$q_l = \frac{k}{\mu}\frac{\partial p_l}{\partial x}$	(Darcy's law)
Constant pressure filtration	
$\mu s\rho\overline{(1-\bar{m}s)^{-1}[\alpha_{av}]_{p_{s_m}}}\frac{V^2}{2} + \mu R_m V = p_0 t$	[6]
Constant rate filtration	
$q_{t_m} = Q, \qquad V = QT$ $P_0 = \mu Q\{s\rho(1-ms)^{-1}[\alpha_{av}]_{p_{s_m}} Qt + R_m\}$	[9]
Pressure drop across filter cake	
$\frac{\Delta p_c}{P_0} = \frac{\mu s\rho\overline{(1-\bar{m}s)^{-1}[\alpha_{av}]_{p_{s_m}}}V}{\mu s\rho\overline{(1-\bar{m}s)^{-1}[\alpha_{av}]_{p_{s_m}}}V + \mu R_m}$	[10]
Compressive stress profile	
$\frac{p_s}{P_a} = \left\{1 + (1-\frac{x}{L})[(1+\frac{\Delta p_c}{P_a})^{1-\delta} - 1\right\}^{\frac{1}{1-\delta}} - 1$	[1]
Solidosity profile	
$\frac{\varepsilon_s}{\varepsilon_s^0} = \left\{\left[(1+\frac{\Delta p_c}{P_a})^{1-\delta} - 1\right](1-\frac{x}{L}) + 1\right\}^{\frac{\beta}{1-\delta}}$	[1]

1.2 THE KOZENY-CARMAN EQUATION

The Kozeny-Carman equation can be used in fluid flow through packed beds. It is based on the conventional theory and extended with experiments at constant pressure. For laminar flow in straight tubes, according to the Hagen-Poiseuille (H-P) equation,

$$\Delta p_s = \frac{32 L \bar{V} \mu}{D^2} \tag{1.2.1}$$

where $\Delta p_s$is the pressure loss, L is the length of pipe, μ is the dynamic viscosity, $\bar{V}$ is the average velocity in the channels, and D is the diameter of the tube. In order to determine an effective tube diameter (D_{eq}) that mimicks the pores within a cake, the surface area for n monomodal tubes should be equal to the surface-volume ratio times the particle volume:

$$n\pi D_{eq} L = \frac{A_{cs} L (1-\varepsilon) 6}{\Phi_s D_p} \tag{1.2.2}$$

where D_p is the particle diameter, Φ_s is the sphericity, A_{cs} is the cross-sectional area of the bed. Similarly, the void volume should be equal to the total volume of tubes.

$$A_{cs} L \varepsilon = \frac{1}{4} n\pi D_{eq}^2 L \tag{1.2.3}$$

Combining to provides the equation for D_{eq}:

$$D_{eq} = \frac{2}{3} \Phi_s D_p \frac{\varepsilon}{1-\varepsilon} \tag{1.2.4}$$

The average volume of channels is proportional to the superficial velocity ($\bar{V}_0$) and inversely proportional to the porosity:

$$\bar{V} = \frac{\bar{V}_0}{\varepsilon} \tag{1.2.5}$$

where ε is the porosity. Adding a correction factor, λ, to represents the fact that channels are tortuous instead of straight and parallel. Combining this modified H-P equation we get

$$\frac{\Delta p}{L} = \frac{72\lambda \bar{V}_0 \mu}{{\Phi_s}^2 D^2} \frac{(1-\varepsilon)^2}{\varepsilon^3} \tag{1.2.6}$$

The correction factor (λ) is typically taken as an empirical number equal to 2.1 so that we obtain [11]:

$$\frac{\Delta p}{L} = \frac{150\bar{V}_0 \mu}{{\Phi_s}^2 D^2} \frac{(1-\varepsilon)^2}{\varepsilon^3} \tag{1.2.7}$$

This indicates that the flow rate is proportional to the ultimate pressure drop and inversely proportional to the fluid viscosity. This equation is similar to Darcy's law; therefore, it does not fit when the cake has high porosity, non-spherical particles, or systems of particles that are multi-disperse [12]. This thesis is focused on modifying the Kozeny-Carman (CK) equation to fit the experiment data in a multi-disperse system.

1.3 MULTI-DISPERSE THEORIES

Cakes of filtration are always composed of multi-sized particles in industry applications. The Kozeny-Carman equation and other theories cannot be directly applied to multi-disperse system. In order to verify the change for a multi-disperse system, the studies during the last decade have been focused on drag forces because the drag forces between fluid and particles are very important in filtration [13]. Koch proposed new relations based on numerical data from simulations [14]. Van der Hoef determined the drag forces of particles in bi-sized spheres in 2005 [15]. Yin and Sundaresan generated a fluid-particle drag forces equation for binary and ternary systems [16]. Because these works were based on very loosely packed beds, the equations may not work well in dense systems. Based on previous works, Rong organized the

relationship between fluid and particles more accurately and reasonably [13]. However, Rong and coworkers assumed that the particles remained stationary when the fluid flowed through them and used very low pressure during the experiment and simulation. In this thesis, the aim is to modify the Kozeny-Carmen equation for a multi-disperse system with a high operating pressure.

1.4 COMPUTATIONAL MODELS

In this section we discuss two modeling techniques that are well suited for the study of fluid-particle filtration. The discrete element method (DEM) is a well-known technique for the calculation of mechanical forces between particles as well as their subsequent motion. The Lattice Boltzmann Method (LBM) is a Lagrangian fluid modeling technique that can easily handle the intricate boundaries that arise in systems of particles (that can have disparate sizes and/or shapes).

1.4.1 DEM simulation

The discrete element method (DEM), which was pioneered by Cundall in 1971, is a numerical method that is used to compute the physic properties of an extensive number of particles [17]. DEM is widely used in simple models of particle interactions because it models materials as an assemblage of discrete particles. It calculates the interaction forces between these particles based on Newton's law. Then it determines how the motion of each particle would change based on the calculated forces. DEM simulation can be run with desired initial conditions, such as the number

of particles, particle diameter, and particle size distribution, for multi-disperse systems. Because DEM can be used to simulate the physical locations of each particle in the model, one method of coupling the DEM and Lattice Boltzmann Method (LBM) techniques is to use the result of a DEM as the initial particle/boundary locations for the LBM [18].

1.4.2 LBM simulation

The Lattice Boltzmann Method (LBM) is a computational model that is widely used in designing models of the physic properties of fluid flow, such as flow rate. LBM is based on the fact that individual molecules compose the fluid and the total behavior of the fluid can be calculated by summing the behavior of each individual molecule [19]. In this thesis, the DEM is used to simulate packed cakes to verify the changes of cake structure in different particle size distributions. Therefore, the simulated results can represent the void size distribution and compare different void size distributions with different particle size distributions. Further work should be done with LBM simulation in order to verify the effect of fluid in different particle size systems.

2.0 FILTRATION EXPERIMENTS

As we assume that applying the Kozeny-Carman equation to multi-disperse systems can result in significant errors, we assess the utility of this equation for application to systems that include poly-disperse particles at moderate fluid pressure. It is important to introduce appropriate experimental techniques in order to determine the difference. As mentioned above, there are different types of filters and operation methods. In this thesis, a Nutsche Filter, which is a cake filter and performs filtration at constant operating pressure, was chosen for the experiments, as shown in Figure 1. Constant pressure filtration is used with a cake that is composed of glass beads with regular, smooth surfaces. The viscous liquid used for the fluid phase in this thesis is pure glycerol.

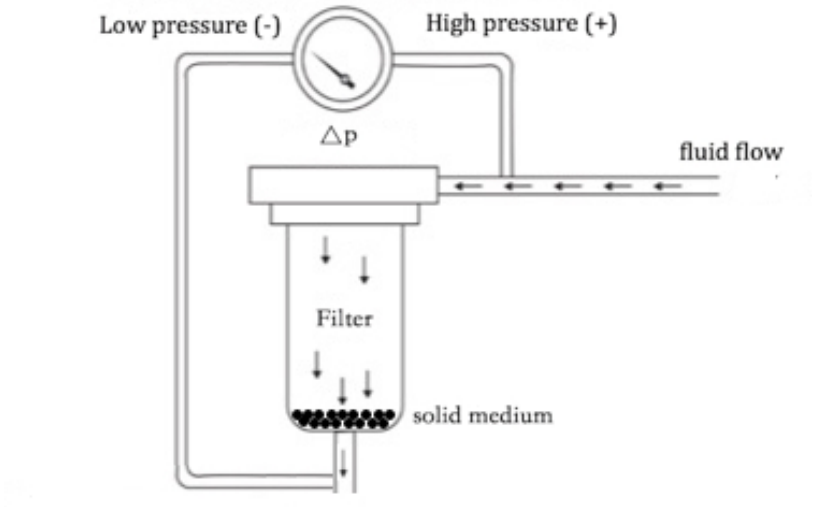

Figure 1. Chart of filtration experiment (Chose a pressure nutsche filter with steam jacket)

The process for each filtration experiment was as follows:

1. Fix filter paper cloth at the bottom of the filter.
2. Pour a known volume and mass of dry glass beads into the filter.
3. Tap the outside chamber several times until the particles have settle evenly.
4. Pour the fluid into the chamber; make sure the structure of solid phase is not destroyed.
5. Apply a known pressure into the filter.
6. Allow the fluid flow through the filter continuous into a beaker, which posited on a scale.
7. Calculate the mass of fluid collected every 30 seconds.
8. Run six times for each cake with six different operating pressures.

We can read the pressure (p) from the vacuum gauge during the experiment. The ultimate pressure drop (Δp) is the pressure in the filter minus the atmospheric pressure:

$$\Delta p = p - p_a \tag{2.0.1}$$

The superficial velocity ($\overline{V_0}$) can be calculated by measuring the accumulated mass of filtered fluid (m_l) as a function of time:

$$\overline{V_0} = \frac{m_l}{\rho S} \tag{2.0.2}$$

where ρ is the density of the fluid, and S is the area of the cake. The volume of the cake (V) is measured by a graduated cylinder， which can calculate the cake thickness (L):

$$L = \frac{V}{S} \tag{2.0.3}$$

The porosity is the fraction of void space in a material. It is determine by the volume of that cake and the mass of added water (m_w). In this thesis, we measured cake volume and cake weight, and then added distilled water until the base of the meniscus of the water liquid was level with the top surface of the solid. The mass of the added water can be calculated by subtracting the

cake weight from the total weight. The porosity could be calculated. As the pressure dropped, the cake thickness, porosity of the cake, diameter of particles, viscosity of the fluid were known, the predicted flow rate could be calculated.

$$\varepsilon = \frac{V}{m_w/\rho_w} \tag{2.0.4}$$

In the following sections we report the raw data obtained from our filtration experiments. Analysis and discussion of these results are largely reserved for Chapter 3.0 .

2.1 FILTRATION IN NARROW SIZE DISTRIBUTION

In order to verify the influence of different multi-disperse systems on the predicted flow rate based on the Kozeny-Carman equation, we chose different size ranges of glass beads with size from 50μm to 100μm. For narrow size distribution in this thesis, the difference between particle sizes should be less than 15μm. Experiments were run using five different particle size distributions and six operating pressures. The cake thicknesses were near 0.5cm and other factors were kept constant. Under these varying operating conditions, the predicted flow rate was determined using the Kozeny-Carman equation, as shown in Table 2.

Table 2. Experiments: predicted flow rate, empirical flow rate in different narrow size distribution

Particle size (μm)	Pressure drop (Pa)	Predicted flow rate (m/s)	Empirical flow rate (m/s)
53-63	76500	5.42E-05	6.02E-05
	124000	8.78E-05	1.05E-04
	174000	1.23E-04	1.40E-04
	222000	1.57E-04	1.86E-04
	268500	1.90E-04	2.15E-04
	308000	2.18E-04	2.49E-04
63-75	82500	9.24E-05	1.06E-04
	124000	1.39E-04	1.56E-04
	183000	2.05E-04	2.24E-04
	227500	2.55E-04	2.84E-04
	269500	3.02E-04	3.33E-04
	314000	3.52E-04	3.88E-04
75-90	87000	2.81E-05	2.92E-05
	142500	4.61E-05	4.84E-05
	181000	5.86E-05	5.87E-05
	230000	7.44E-05	7.23E-05
	283500	9.17E-05	9.27E-05
	316000	1.02E-04	1.04E-04
90-106	74000	5.34E-05	5.46E-05
	131500	9.50E-05	1.00E-04
	177500	1.28E-04	1.37E-04
	219000	1.58E-04	1.70E-04
	264000	1.91E-04	2.08E-04
	295000	2.13E-04	2.39E-04

As shown in the data above, the empirical data is quite similar to the predicted data in these narrow size distributions in thin cakes no matter how particle sizes change. Also, the cake thickness may also influence the flow rate. In order to verify this influence, experiments were run using three different cake thicknesses and six operating pressure with particle sizes between

90 and 106μm. In addition, other factors were kept constant. We compared the predicted flow rates to the empirical flow rates, as shown in Table 3. The empirical data is still quite similar to the predicted data no matter how the cake thickness was changed.

Table 3. Experiments: predicted flow rate, empirical flow rate in different cake thickness (particle size 90-106μm)

Cake thickness (cm)	Pressure drop (Pa)	Predicted flow rate (m/s)	Empirical flow rate (m/s)
0.54	74000	5.34E-05	5.46E-05
	131500	9.50E-05	1.00E-04
	177500	1.28E-04	1.37E-04
	219000	1.58E-04	1.70E-04
	264000	1.91E-04	2.08E-04
	295000	2.13E-04	2.39E-04
2.50	77500	1.76E-05	1.92E-05
	148000	3.36E-05	3.57E-05
	192500	4.37E-05	4.97E-05
	227500	5.17E-05	5.71E-05
	275000	6.25E-05	6.86E-05
	350000	7.95E-05	8.34E-05
4.91	78500	6.93E-06	7.62E-06
	137500	1.21E-05	1.29E-05
	171500	1.51E-05	1.57E-05
	213500	1.88E-05	2.03E-05
	269000	2.38E-05	2.46E-05
	307500	2.70E-05	2.92E-05

2.2 FILTRATION IN WIDE SIZE DISTRIBUTION

The differences between the predicted flow rates and the empirical flow rates are quite similar in narrow size distribution, regardless of particle size and cake thickness. This means that the

Kozeny-Carman equation is suitable for use in narrow size distribution system. We chose larger size ranges, wide size distribution, with sizes from 50μm to 210μm. In this thesis, wide size distribution is defined as when the difference between particle sizes is greater than 15μm. Experiments similar to those in Chapter 2.1 were conducted. The empirical results and predicted flow rates based on the Kozeny-Carman equation are shown in Table 4.

Table 4. Experiments: predicted flow rate, empirical flow rate in different wide size distribution

Particle size (μm)	Pressure drop (Pa)	Predicted flow rate (m/s)	Empirical flow rate (m/s)
50-75	78000	7.91E-06	1.65E-05
	136000	1.26E-05	3.16E-05
	176500	1.63E-05	4.18E-05
	216000	2.18E-05	5.33E-05
	266000	2.70E-05	6.88E-05
	308000	3.12E-05	8.36E-05
50-100	90000	1.40E-05	4.55E-05
	128000	1.99E-05	5.07E-05
	181500	2.82E-05	7.00E-05
	225000	3.50E-05	8.58E-05
	282000	4.38E-05	1.04E-04
	310000	4.82E-05	1.18E-04
75-100	82500	1.99E-05	5.91E-05
	126000	3.07E-05	1.03E-04
	172000	4.19E-05	1.06E-04
	224000	5.46E-05	1.57E-04
	235000	5.73E-05	1.60E-04
	298000	7.26E-05	2.10E-04
150-177	76000	5.45E-05	9.88E-05
	131500	9.42E-05	1.79E-04
	171500	1.23E-04	2.31E-04
	217500	1.56E-04	2.94E-04
	272000	1.95E-04	3.53E-04
	311000	2.23E-04	4.97E-04

Table 4 (continued).

180-210	84500	6.91E-05	1.10E-04
	127500	1.04E-04	1.69E-04
	185500	1.52E-04	2.56E-04
	219000	1.79E-04	3.07E-04
	281500	2.29E-04	4.01E-04
	308500	2.52E-04	4.54E-04

As shown by the data above, the empirical data is quite different from the predicted data for the wide size distributions. In order to verify the influence of cake thickness, experiments

Table 5. Experiments: predicted flow rate, empirical flow rate in different cake thickness (particle size 50-100μm)

Cake thickness (cm)	Pressure drop (Pa)	Predicted flow rate (m/s)	Empirical flow rate (m/s)
0.53	79000	2.31E-05	4.49E-05
	128500	3.95E-05	7.62E-05
	193000	6.24E-05	1.16E-04
	239500	7.86E-05	1.60E-04
	278000	9.12E-05	1.68E-04
	311500	1.01E-04	1.99E-04
2.16	90000	1.40E-05	4.55E-05
	128000	1.99E-05	5.07E-05
	181500	2.82E-05	7.00E-05
	225000	3.50E-05	8.58E-05
	282000	4.38E-05	1.04E-04
	310000	4.82E-05	1.18E-04
5.10	154000	8.49E-06	3.37E-05
	190500	1.05E-05	4.24E-05
	241000	1.33E-05	5.08E-05
	277500	1.53E-05	5.67E-05
	327500	1.81E-05	6.70E-05
	409000	2.26E-05	8.86E-05

were run using three different cakes with particle size of 50 to 100μm. Additionally, other factors were kept constant. Predicted flow rates were compared to the empirical flow rates that were actually obtained, as shown in Table 5.

2.3 FILTRATION IN BINARY DISTRIBUTION

Based on the results presented in Chapters 2.1 and 2.2, the Kozeny-Carman can only be used to predict flow rate in filtration experiments with narrow size distribution. However, the cake structure is very complicated and difficult to simulate. Binary mixing was chosen in order to specify the effects of particle size distribution on the filtration process. The procedure for each filtration experiment is similar to the procedure above. However, before the filtration, a known volume of small particles and large particles were agitated with a mixer by add a little water to create a roughly homogeneous binary mixture and then the cake was allowed to dry under forced air flow. Experiments were run using five different size ratios and six operating pressures. The cake thicknesses were near 2cm and other factors were kept constant. From these varying operating conditions, we predicted the flow rate using the Kozeny-Carman equation with particle averaging methods based on Rong's work [13]. His method to apply the equation in binary mixing is to treat a multi-disperse system as a mono-disperse system by using an average diameter, the harmonic mean diameter, as shown [20].

$$d_{HM} = \frac{n}{\sum_{i=1}^{n} \frac{1}{d_i}} \tag{2.3.1}$$

The harmonic mean is one of several kinds of average that can be expressed as the reciprocal of the arithmetic mean of the reciprocals, and it is appropriate for situations if the average rate is desired. The harmonic mean diameter is a mathematical expression that is calculated using the

Table 6. Experiments: predicted flow rate, empirical flow rate in different cake thickness for binary distribution

Particle size (μm)	Pressure drop (Pa)	Predicted flow rate (m/s)	Empirical flow rate (m/s)
82:98	79000	1.23E-05	2.24E-05
	137000	2.14E-05	3.90E-05
	166000	2.59E-05	4.87E-05
	216000	3.38E-05	6.54E-05
	255500	3.99E-05	7.33E-05
	298000	4.66E-05	8.65E-05
100:200	104000	4.23E-05	9.61E-05
	145000	5.90E-05	1.25E-04
	196000	7.98E-05	1.67E-04
	251500	1.02E-04	2.16E-04
	281500	1.15E-04	2.38E-04
	330000	1.34E-04	2.75E-04
100:500	70000	3.90E-04	4.74E-04
	100000	5.57E-04	6.07E-04
	108000	6.02E-04	6.48E-04
	147500	8.22E-04	8.62E-04
	168500	9.39E-04	9.43E-04
	192500	1.07E-03	1.02E-03
163:500	77000	1.82E-04	2.12E-04
	129000	3.06E-04	3.60E-04
	174000	4.12E-04	4.69E-04
	229000	5.42E-04	5.88E-04
	267500	6.34E-04	6.60E-04
	313500	7.43E-04	7.48E-04

distribution function. By using the harmonic mean diameter, the Ergun equation (or Darcy's law) have been shown to reasonably estimate the pressure drop for multi-disperse system at low pressures [21].The experiment results and predicted flow rates from Kozeny-Carman equation are shown in Table 6.

3.0 DISCUSSION

In order to verify the utility of the Kozeny-Carman equation in a poly-disperse system, empirical flow rate was compared to predicted flow rate under the same operating pressure. Curve Fitting Toolbox™ (from MATLAB, command: cftool) was used to evaluate the goodness of fit between data and predicted line. The goodness-of-fit statistics used in this thesis were the Sum of Squares Due to Error (SSE), R-square and Root Mean Squared Error (RMSE). SSE measured the total deviation of data from the fit model to data:

$$SSE = \sum_{i=1}^{n} (y_i - \hat{y}_i)^2 \tag{4.0.1}$$

where y_i is the empirical flow rate and $\hat{y}_i$ is the predicted flow rate from models. A smaller value of SSE points out that the model fit will be more effective for prediction. R-square is defined as the ratio of the Sum of Squares of the Regression (SSR) and the Total Sum of Squares (SST)

$$SSR = \sum_{i=1}^{n} (\hat{y}_i - \bar{y})^2 \tag{4.0.2}$$

$$SST = \sum_{i=1}^{n} (y_i - \bar{y})^2 \tag{4.0.3}$$

$$R - square = \frac{SSR}{SST} = 1 - \frac{SSE}{SST} \tag{4.0.4}$$

where $\bar{y}$ is the mean of the empirical data. R-Square evaluates how well data fit models; a R-Square of 1 means the predicted line from model fits the data perfectly.

3.1 DISCUSSION OF NARROW SIZE DISTRIBUTION

Figure 2 illustrates how well the empirical flow rates matched the predicted flow rates made by the Kozeny-Carman equation in narrow size distribution samples. Although the flow rates predicted by the Kozeny-Carman equation were consistently a little lower than the empirical results in these narrow size distribution samples, the error between the empirical data and predicted data, as calculated by the percent error equation, is less than 15% (see by Table 7). Moreover, the goodness-of-fit statistics also illustrate Kozeny-Carman models are useful to predict the flow rate in narrow disperse system as the values of R-Square (see by Table 7) are consistently larger than 0.95.

Because cake thickness can influence flow rate, Figure 3 shows how well the empirical flow rates fit with the predicted flow rates for different thicknesses and with the same size distribution: 90-106μm. The flow rate decreased significantly with the increase of cake thickness in Figure 3. However, the errors between the empirical data and the predicted data are still small, and value of R-Square are still larger than 0.95 (see by Table 8). This quantitatively confirms that the Kozeny-Carman equation can be applied in multi-disperse systems with very narrow size distribution.

Table 7. Experiment results: different between predicted flow rate and empirical flow rate in vary sizes (narrow size distribution)

Size (μm)	Error	SSE	R-square	RMSE
53-63	13.11%	3.700e-10	0.9808	8.602e-06
63-75	9.36%	4.015e-10	0.9930	8.961e-06
75-90	3.21%	1.205e-11	0.9969	1.552e-06
90-106	7.01%	3.946e-10	0.9832	8.884e-06
500	5.25%	1.194e-10	0.9655	4.887e-06

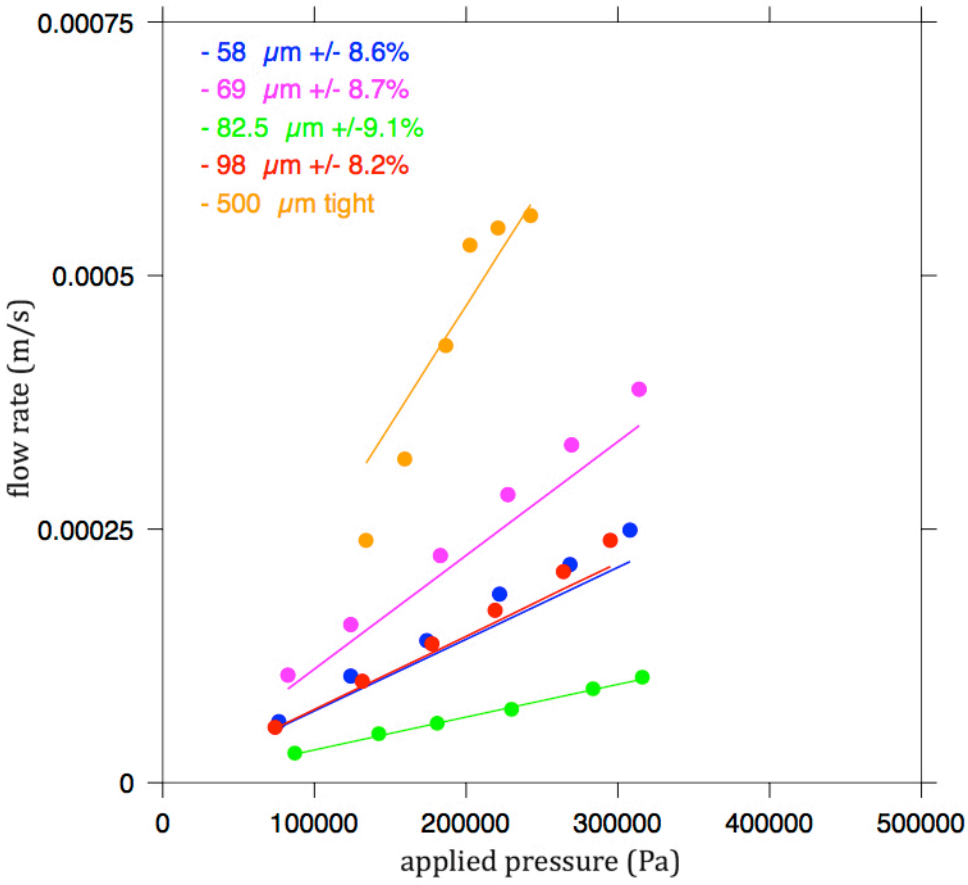

Figure 2. The relationship between operating pressure and flow rate with narrow size distribution particles (line: predicted flow rate, point: empirical flow rate)

Table 8. Experiment results: different between predicted flow rate and empirical flow rate in vary cake thicknesses (particle size 90-106µm)

Cake thickness (cm)	Error	SSE	R-square	RMSE
0.54	7.01%	3.946e-10	0.9832	8.884e-06
2.51	9.87%	1.242e-10	0.9528	4.550e-06
4.91	7.81%	1.762e-12	0.9944	5.936e-07

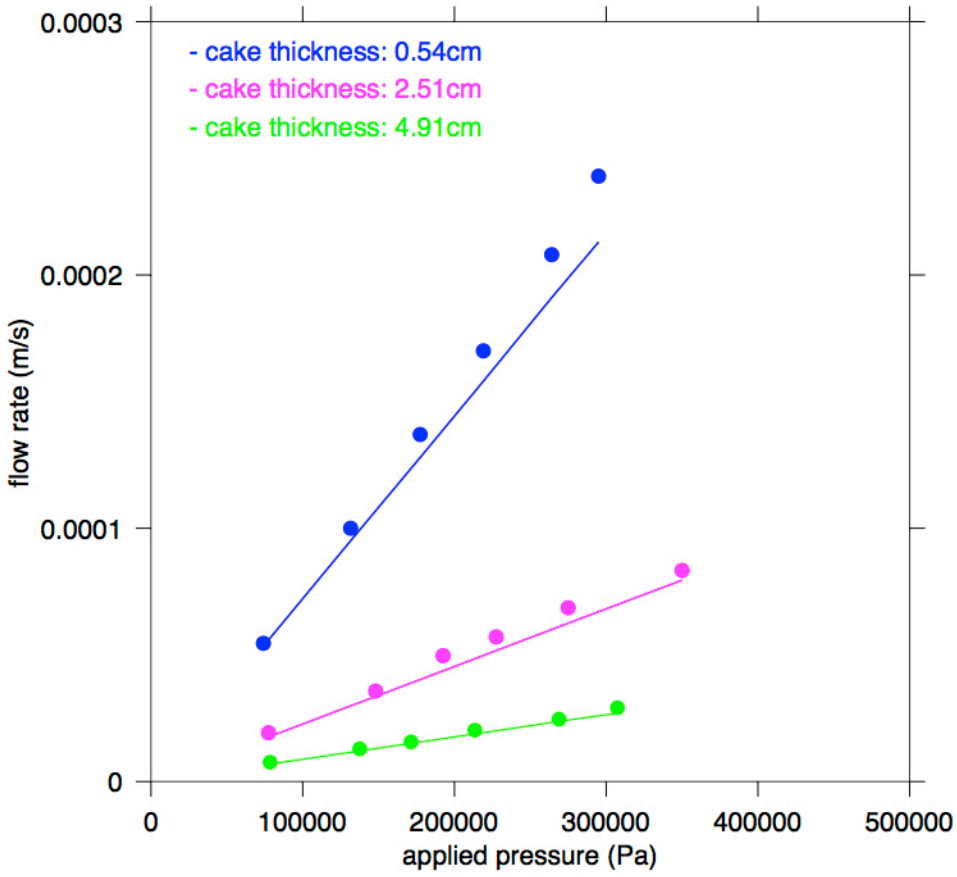

Figure 3. The relationship between operating pressure and flow rate in different thickness with 90-106µm particles (line: predicted flow rate, point: empirical flow rate)

3.2 DISCUSSION OF WIDE SIZE DISTRIBUTION

Figure 4 illustrates how well the empirical flow rates aligned with the predicted flow rates based on the Kozeny-Carman equation for wide size distribution samples. The flow rates predicted by the Kozeny-Carman equation were consistently much lower than the flow rate obtained experimentally, and the error between the empirical data and the predicted data was much larger than in the narrow size distribution samples (see by Table 11). Because the error is always larger than 50% and values of R-Square (see by Table 11) are always smaller than 0.80, the goodness-of-fit statistics confirm that Kozeny-Carman models are not well suited to predict flow rates in widely dispersed systems. Even if we tried to fit the predicted result with the empirical one, a much higher mean diameter is found which is ridiculous as shown in Table 9.

Table 9. Fit size in wide size distribution

Size (μm)	Fit size (μm)
50-75	92
50-100	120
75-100	171
150-177	223
180-210	239

Figure 5 shows how well the empirical flow rates aligned with the predicted flow rates for cakes of different thicknesses and with the same size distribution: 50-100μm. The errors between the empirical data and the predicted data are increased by the increase of cake thickness (see by Table 12). Also, even if we introduce a fit mean diameter 120 μm, we still need to modify the tortuosity to keep the agreement as shown in Table 10.

Table 10. Fit tortuosity in wide size distribution (50-100μm)

Cake thickness (cm)	Fit λ
0.53	2.78
2.16	2.08
5.01	1.46

We assumed that the increase of error in this situation is caused by the deformation of cake structure with wide size distribution. Because the diameter of particles are quite similar to each other in narrow size distribution samples, we can treat the cake structure as a mono-disperse system, but as the size distribution gets larger, the cake structure changes, and the particles in the cake cannot form ordered packings [22]. The large error between the empirical results and the predicted results demonstrates the influence of flow rate by changing the void volume of the cake. As the void volume becomes larger, caused by the formation of channels, the flow rate can be obviously increased.

Table 11. Experiment results: different between predicted flow rate and empirical flow rate in vary sizes (wide size distribution)

Size (μm)	Error	SSE	R-square	RMSE
50-75	133.42%	1.246e-09	0.5871	1.579e-05
50-100	145.32%	1.237e-09	0.7052	1.573e-05
75-100	62.47%	6.048e-09	0.5778	3.478e-05
150-177	71.52%	3.133e-08	0.6800	7.916e-05
180-210	88.21%	1.903e-08	0.7823	6.169e-05

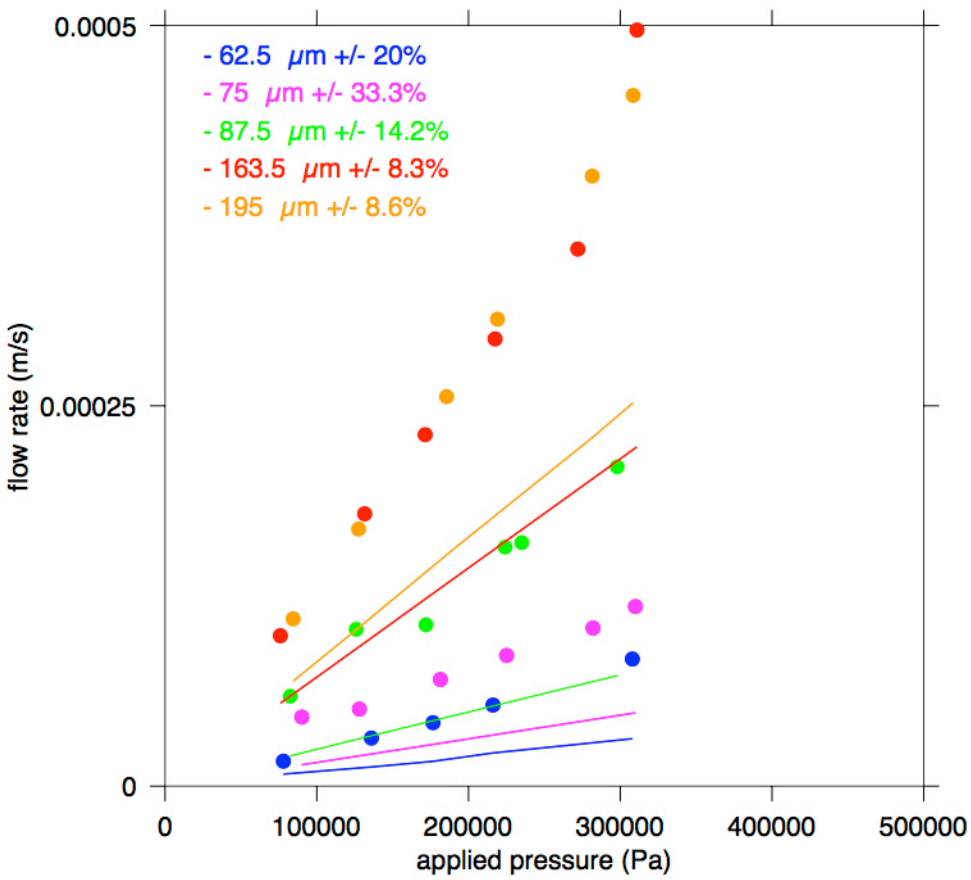

Figure 4. The relationship between operating pressure and flow rate with wide size distribution particles (line: predicted flow rate, point: empirical flow rate)

Table 12. Experiment results: different between predicted flow rate and empirical flow rate in vary cake thicknesses (particle size 50-100μm)

Cake thickness (cm)	Error	SSE	R-square	RMSE
0.53	102.87%	4.218e-09	0.7575	2.905e-05
2.16	145.32%	1.237e-09	0.7052	1.573e-05
5.01	256.59%	1.028e-09	0.4566	1.434e-05

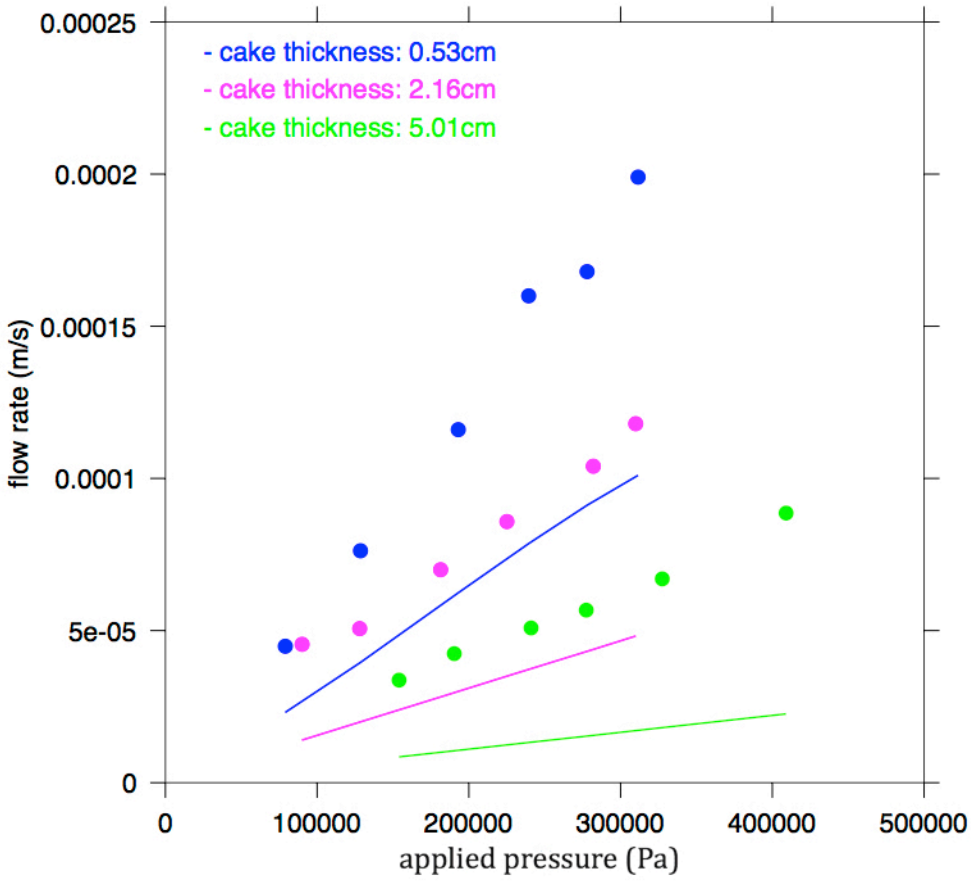

Figure 5. The relationship between operating pressure and flow rate in different thickness with 50-100μm particles (line: predicted flow rate, point: empirical flow rate)

3.3 DISCUSSION OF BINARY DISTRIBUTION

As shown in Table 13, the errors between the empirical data and the predicted data are quite small for $R_{s/l}$=0.20 and $R_{s/l}$=0.33. However, the errors between empirical data and predicted data are much larger for $R_{s/l}$=0.50 and $R_{s/l}$=0.84. Therefore, the flow rate for a constant pressure filtration cake can be predicted by the Kozeny-Carman equation for small size ratios ($R_{s/l}$<0.50), and it is inaccurate for large size ratios ($R_{s/l}$≥0.50) (as shown by Figure 6). As previously explained, empirical results are influenced by particle distribution. Based on the work by Lash

[22], for binary systems, particles with $R_{s/l}$<0.50 can be packed efficiently, so the cakes have a tight distribution of void sizes; in contrast, particles with $R_{s/l} \geq 0.50$ cannot form ordered packings (see by Appendix A). For $R_{s/l} > 0.3$, a tendency for small particles to form a layer on the substrate below the binary-disperse system was observed and more small particles were placed around the edges, also shown a disordered packing [22].

Because the particles cannot form ordered packings for $R_{s/l} \geq 0.50$, we hypothesize that some voids are expanded by this disordered packing which can lead to channel formation and ultimately explain the much higher flow rate that is observed during filtration. Alternatively, for particles with a size ratio $R_{s/l} < 0.50$, we expect that the ordered packing that is achieved will behave much like a monomodal particle system (with a narrow size distribution). As a test of these two hypotheses, we endeavor to examine the void distributions observed in packings of binary systems in the next Chapter.

Table 13. Experiment results: different between predicted flow rate and empirical flow rate in different size ratios

Size ratio	Error	SSE	R-square	RMSE
0.84	87.71%	6.128e-10	0.7803	1.107e-05
0.50	110.85%	5.821e-09	0.7543	3.412e-05
0.33	11.17%	1.957e-09	0.9901	1.978e-05
0.20	4.86%	1.087e-08	0.9526	4.663e-05

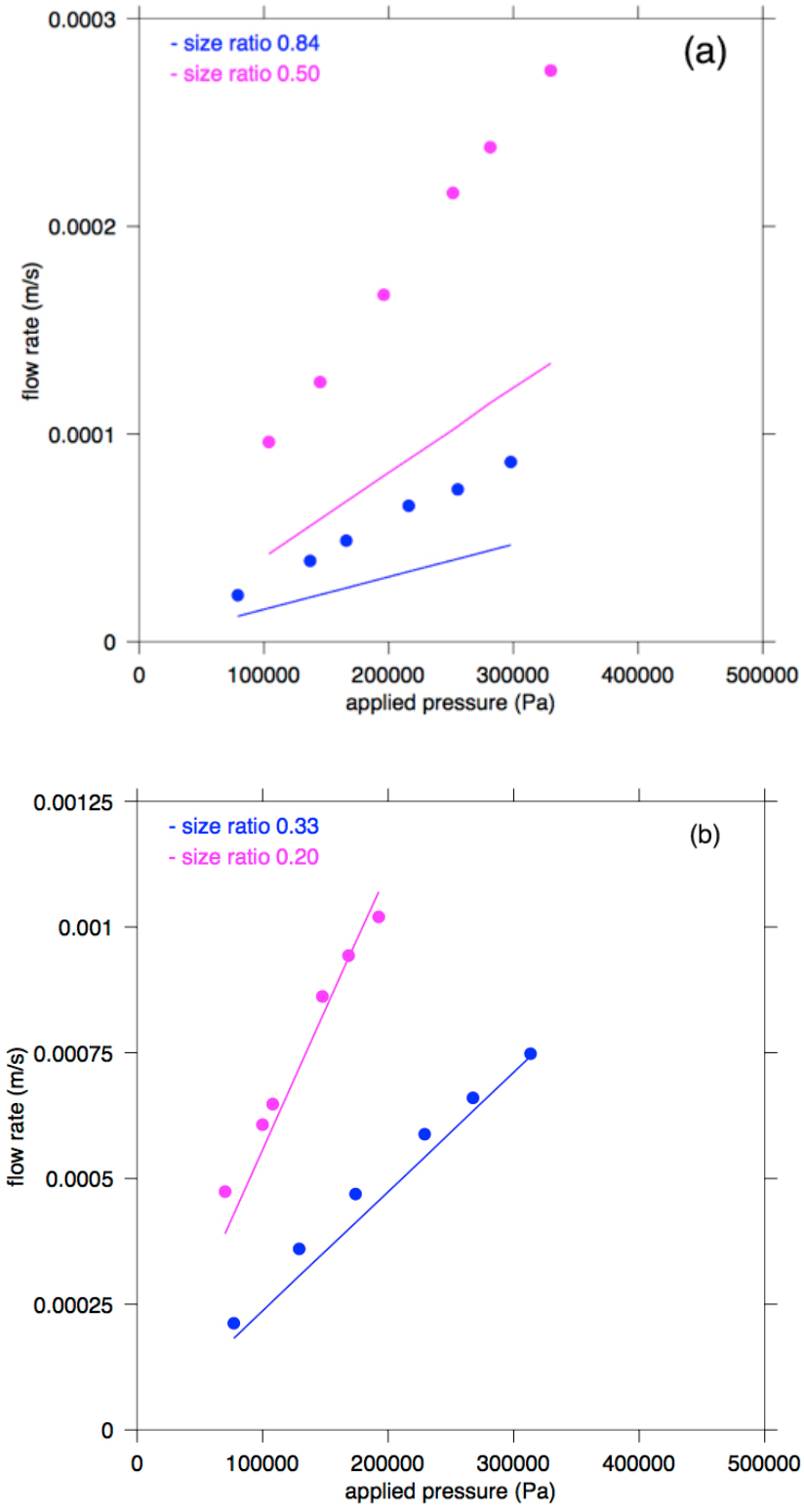

Figure 6. The relationship between operating pressure and flow rate with binary mixing particles (line: predicted flow rate, point: empirical flow rate)

4.0 SIMULATION

4.1 INTRODUCTION OF SIMULATION

In a medium that is composed of spherical particles, it is difficult to interpret because the forces or stresses inside the medium cannot be measured and only can be estimated from the boundary conditions, which is non-linear and hysteretic. These complicated forces led to the development of models. The analytical models for unique packing made from Duffy and Mindlin (1957). The analytical models for random packing made from Digby (1981). These models are limited in spherical particles with uniform size; especially loading path and little deformation can be occurred. The physical models, or called as typically photo-elastic models made from Dantu (1957). These models are time-consuming on and lack flexibility to run multiple test [23].

Theoretical models should be validated by physical experiments. Unfortunately, either theoretical or experimental methods are based on the assumption of material behavior like the macroscopic stress from the boundary conditions. So the reliability to used information obtained at the boundary conditions is unknown. As a result, a more powerful way to modeling granular media is numerical techniques. In this modeling, boundary conditions can be controlled or replaced by a periodic cell; forces can be measured by different changes of any parameter. So we chose the distinct element method (DEM) to model the filtration cake.

4.2 INTRODUCTION OF DEM SIMULATIONS

As introduced in Chapter 1.4, DEM includes all numerical methods handling the problem domain as a combination of independent elements. To simulate a granular material, a critical component is the formulation for representing contacts between individual particles with mathematical and numerical techniques. The basic theory of this method is the Newton's law. Cundall and Strack first developed this method and considered the stress on the granular media generated by external forces and friction or elastic impacts between two spheres of particles [24]. However, they didn't consider forces of intermolecular or inter-particle. Then DEM was introduced on the micrometer scale by account for particle interactions in fine particulate systems [25]. Dong especially worked on mechanisms of the cake build-up in filtration and sedimentation, which can illustrate the influence of material properties on the cake structure and the contact force network inside the filter cake [26].

In common, forces acting on the particles can be divided into two parts: primary forces that due to external effects and inter-particle interactions formed in the system; contact forces that associated with the actual strains within the inter-particle contact regions [27]. Primary forces can also be divided into external forces that work on particle itself which depend on their absolute position in the model and interaction forces between two nearby particles.

4.3 COMPUTATIONAL ALGORITHMS OF DEM SIMULATIONS

As above, DEM is a method to solve Newton's laws of motion for each discrete elements allowing for all degrees of freedom to describe the physic properties of each particle individually in the system depending on time t [27]:

$$m_i \frac{d\vec{v_i}}{dt} = \vec{F_i} \tag{4.3.1}$$

$$I_i \frac{d\vec{\omega_i}}{dt} = \vec{T_i} \tag{4.3.2}$$

where v_i is the transitional velocity of particle i, m_i is the mass of particle i, ω_i is the rotational velocity of particle i, I_i is the moment of inertial of particle i. The force $\vec{F_i}$ is the force that acting on the particle i as shown:

$$\vec{F_i} = \sum \left(\vec{F}_{vdWm,ij} + \vec{F}_{n,ij} + \vec{F}_{t,ij}\right) + \vec{F}_{g,b} \tag{4.3.3}$$

$\vec{T_i}$, the rotation phenomena are not considered. $F_{g,b}$ is the gravity and buoyancy forces that calculated by:

$$\vec{F}_{g,b} = \frac{\pi}{6} d^3 \Delta\rho_{sl} \vec{g} \tag{4.3.4}$$

where $\Delta\rho_{sl}$ is the difference of density between particle and the liquid phase, g is the gravitational acceleration, d is the particle diameter. Particle and particle contacts can be treated as a hard-sphere approximation or a soft-sphere approach [25]. Soft-sphere approach is frequently more useful because collisions in multi-body are shown as a virtual overlapping of the particle spheres [27]. The overlap is calculated from:

$$\lambda = \frac{d_i + d_j}{2} - \left|\vec{r}_{ij}\right| \tag{4.3.6}$$

where r_{ij} is the distance between two particle centers, d_i is the diameter of particle i and d_j is the diameter of particle j. The contact forces during collisions are shown in Figure 7. The normal contact force:

$$\vec{F}_{n,ij}\vec{n}_{ij} = k_n\lambda^{1.5} - \eta_{n,ij}\vec{v}_{rel,n,ij} \tag{4.3.7}$$

where $k_n$is the spring constant in normal direction calculated with:

$$k_n = \frac{|\vec{F}_{max}|}{[d(1-\lambda^*)]^{1.5}} \tag{4.3.8}$$

where λ^* is a defined penetration [28], $\eta_{n,ij}$ is the damping constant in normal direction:

$$\eta_{n,ij} = c_n\sqrt{\frac{9}{2}\left(\frac{m_i m_j}{m_i + m_j}\right)\sqrt{\lambda}k_n} \tag{4.3.9}$$

where c_n is the damping coefficient which is equal to 0.3 [29]. Tangential force in static particles is shown as:

$$\vec{F}_{t,ij} = -k_{t,sta}\Delta x_{t,ij} - \eta_{t,ij}\vec{v}_{rel,t,ij} \tag{4.3.10}$$

where $k_{t,sta}$ is the static spring constant in tangential direction and $\eta_{t,ij}$ is the damping constant in tangential direction:

$$k_{t,sta/dyn} = \frac{\mu_{sta/dyn}}{d(1-\lambda^*)}|\vec{F}_{max}| \tag{4.3.11}$$

$$\eta_{t,ij} = 2\sqrt{\frac{2}{7}\left(\frac{m_i m_j}{m_i + m_j}\right)k_{t,dyn}} \tag{4.3.12}$$

where $\mu_{sta/dyn}$ is the static or dynamic friction coefficient. Tangential forces are changed with the transcending of the static friction and the moving of particles:

$$\vec{F}_{t,ij} = -\mu_{dyn}|\vec{F}_{n,ij}|\vec{t}_{ij}\Delta x_{t,ij} \tag{4.3.13}$$

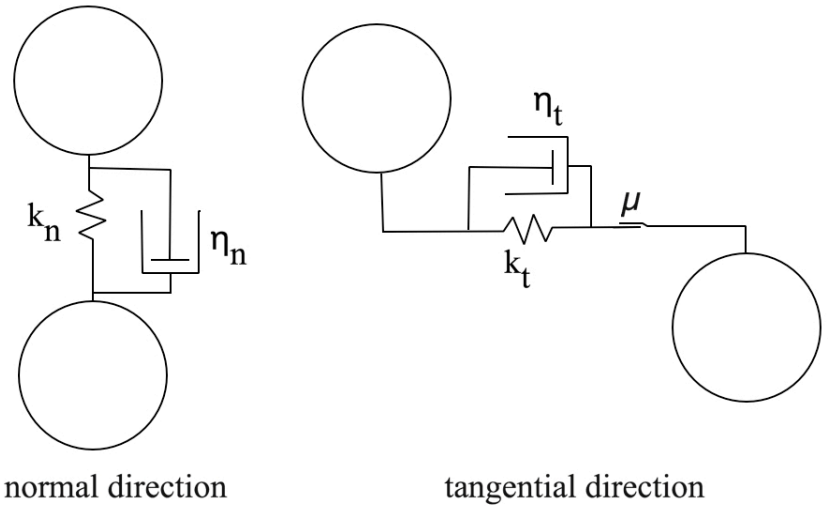

Figure 7. Particle-particle contact models (normal direction: spring and damper; tangential direction: spring, damper and slider) adapted from Ref. [27]

Based on DEM simulation of filtration cake, we can get each particle positions during the process by changing the initial conditions correlated to the physical conditions of the experiments. With the particle positions, the void size distribution of that cake can be represented as discussed in Chapter 5.3. The packed beds in Chapter 5 are simulated layer-by-layer (as shown in Appendix B), random packed beds analysis is shown in Appendix C .

5.0 MODIFIED EQUATION

As we mentioned above, filtration can be influenced by the size ratio of the particles that compose the cake, since different size ratios may form different cake structures. Based on our observations in previous chapter, predicted and empirical results can only be favorably compared for systems that result in well-ordered particle packings, which have a tight distribution of void sizes (or very different means sizes in a binary mixture – size ratios $R_{s/l}$ <0.50). Dramatic disagreement is observed for particle beds that exhibit wide void size distributions or those that forma binary mixture with means that are moderately similar (i.e., size ratio $R_{s/l}$ >0.50). In order to test our hypothesis that ordered packings results in narrow void distributions, while disorder packings lead to wide void distributions,it is critical to determine the void size distribution of the cake. Moreover, in this chapter we propose a modified form of the Kozeny-Carman equation that directly utilizes this void distribution and that we expect will be able to more accurately predict flow behavior. Simulation models from DEM are used to analyse the void size distribution of each simulated cake structure.

5.1 MODIFICATION OF KOZENY-CARMAN EQUATION

We assumed that the increase of flow rate is caused by disorder within the cake structure. This disorder, at a minimum, will lead to the formation of a non-monomodal distribution of effective

void sizes. As such, as a simple first approximation, we intriduce two factors to describe the expansion of the voids as shown in Appedix D. κ is the fraction of expanded voids, and β is the ratio of void sizes. In all of the foloowing equations, we note that the sphericity of glass beads is 1 so that subsequent analysis is simplified (although relaxing this simplification would be trivial).

$$\Phi_s = \frac{6/d_p}{S_p/V_p} = 1 \tag{5.1.1}$$

In order to determine the void tube diameter (D_{eq}) in multi-disperse medium, the surface area for n tubes should be equal to the surface-volume ratio times the particle volume:

$$\kappa n\pi\beta D_{eq}L + (1-\kappa)n\pi D_{eq}L = A_{cs}L(1-\varepsilon)6/D_p \tag{5.1.2}$$

$$\frac{A_{cs}L(1-\varepsilon)6}{D_p} = [\kappa\beta + (1-\kappa)]n\pi D_{eq}L \tag{5.1.3}$$

$$\frac{A_{cs}(1-\varepsilon)6}{D_p} = [\kappa\beta + (1-\kappa)]n\pi D_{eq} \tag{5.1.4}$$

Similarly, the void volume is equal to the total volume of tubes.

$$A_{cs}L\varepsilon = \frac{1}{4}n\pi D_{eq}^2\kappa\beta^2 L + \frac{1}{4}n\pi D_{eq}^2(1-\kappa)\mathrm{L} \tag{5.1.5}$$

$$A_{cs}\varepsilon = [\kappa\beta^2 + (1-\mathrm{K})]\frac{1}{4}n\pi D_{eq}^2 \tag{5.1.6}$$

Combining to provides the equation for D_{eq}:

$$D_{eq} = \frac{2}{3}\frac{\kappa\beta + (1-\kappa)}{\kappa\beta^2 + (1-\kappa)}\frac{\varepsilon}{1-\varepsilon}D_p \tag{5.1.7}$$

Due to the fact that we have now assumed that the packed bed has two mean void size, D_{eq} and βD_{eq}, the actual velocity in each tube is no longer identical. We will take the actual velocity in a normal tube as v, so the actual velocity in an expanded tube should be βv. Then we can achieve the relationship between superficial velocity and actual velocity by match the same volumetric flow rate:

$$A_{cs} \times v_{sup} = \frac{1}{4}\pi n[\kappa\beta^2 v\beta^2 + (1-\kappa)v]D_{eq}^2 \quad (5.1.8)$$

Combining this expression to gives

$$v_{sup} = \varepsilon \times v[\frac{\kappa\beta^4 + (1-\kappa)}{\kappa\beta^2 + (1-\kappa)}] \quad (5.1.9)$$

According to the Hagen-Poiseuille equation:

$$\frac{\Delta \mathrm{p}}{\mathrm{L}} = \frac{32v\mu}{\mathrm{D_{eq}^2}} \quad (5.1.10)$$

Taking u to represent v_{sup}, therefore, we can obtain the modified Kozeny-Carman equation for multi-disperse systems:

$$\frac{\Delta p}{\lambda L} = \frac{72v_{sup}\mu(1-\varepsilon)^2}{{D_p}^2\varepsilon^3}\frac{[\kappa\beta^2 + (1-\kappa)]^3}{[\kappa\beta^4 + (1-\kappa)] \times [\kappa\beta + (1-\kappa)]^2} \quad (5.1.11)$$

Because we assumed that some voids are expanded, so the pathway can be more linear as fluid has more gaps to flow through. As a result, the tortuosity should be decreased. The tortuosity factor λ can be modified base on its definition: tortuosity is the ratio between the length of the real pathway and the distance between two ends. Based on Figure 8, the length of real pathway can be calculated by the equation:

$$L' = D_{eq} + 2D_p \quad (5.1.12)$$

Similarly, the distance between two ends is:

$$L = D_{eq} + D_p \quad (5.1.13)$$

So we can calculate the tortuosity by sum of the normal one and the expanded one,

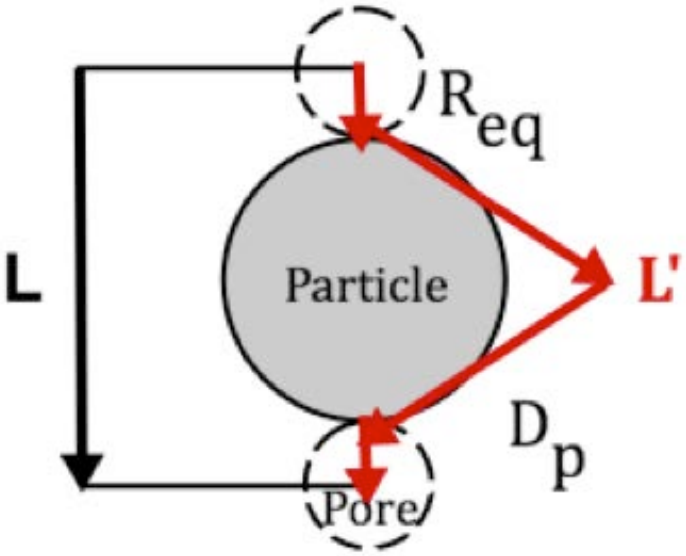

Figure 8. Determination of tortuosity through a particle

$$\lambda_{tot} = (1-\kappa)\lambda_{normal} + \kappa\lambda_{expanded} = (1-\kappa)\frac{D_{eq}+2D_p}{D_{eq}+D_p} + \kappa\frac{\beta D_{eq}+2D_p}{\beta D_{eq}+D_p} \quad (5.1.15)$$

Based on equation, we can calculate the modified tortuosity with the modified factors. It is important to note that, for a mono-modal distribution of voids, this equation predicts a value tortuosity equal to 2.1 (as is typically chosen empirically).

5.2 INTRODUCTION OF DELAUNAY TESSELATION

Voronoi and Delaunay tessellations can be used to describe a cake geometrically. In mathematics, a Voronoi diagram (see Figure 9), also called a Voronoi tessellation, or a Voronoi partition, is a partitioning of a space into regions based on distance to points in a specific subset of the space. In this thesis, the specific subset is the set (P) of the centres of the particles that make up the

assembly. That set of points is specified beforehand and are closer to a given point of P to any other points in the set [30]. The Voronoi diagram of a set of point is due to its Delaunay triangulation.

The Delaunay triangulation in the plane, which is also called Delaunay tessellation, is another fundamental computational geometrical structure. The Delaunay tessellation (DT) is a straight-line dual tessellation of the Voronoi diagram. DT maximizes the minimum angle of all the angles of the triangles in the triangulation, which is obtained by attaching entire pairs of points belongs to in the set P whose Voronoi regions share a common Voronoi edge (see Figure 10) [31].

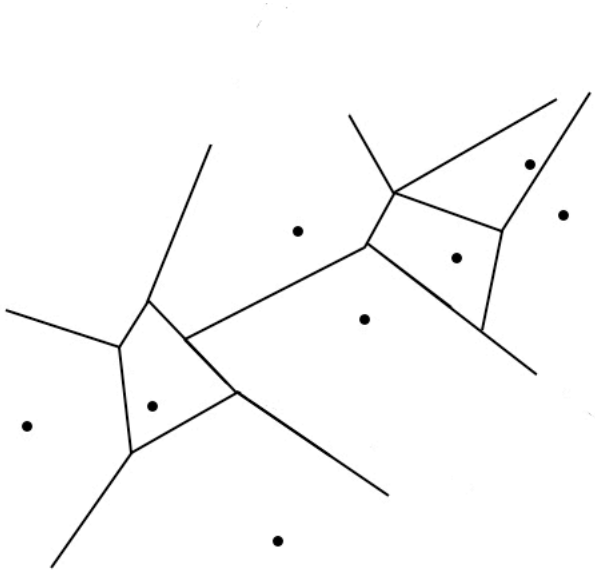

Figure 9. Voronoi diagram for eleven sites in the plane adapted from Ref. [30]

Even though Voronoi tessellation has been commonly used to portray local arrangement in a granular medium [32-34], DT is told to be more appropriate for characterizing and quantifying pore volumes for fluid flow computations [35-37]. A pore in this thesis is defined as the void space inside a Delaunay cell as shown in Figure 11 [38]. Because the positions of the

centres of particles in the cake are known by the DEM, we can determine each void volume based on their positions in MATLAB.

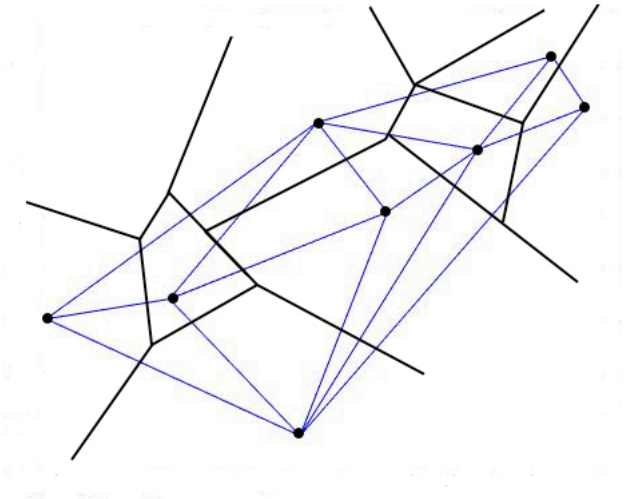

Figure 10. The dual Delaunay triangulation of the Voronoi diagram adapted from Ref. [31]

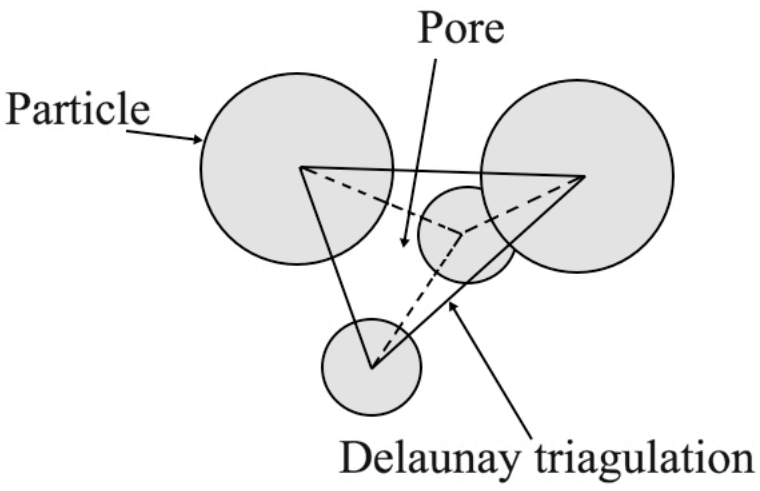

Figure 11. A 3D Delaunay cell (particle size ratio $R_{s/l} = 0.5$): a pore located inside the Delaunay tetrahedron adapted from Ref. [38]

5.3 REPRESENTATION OF THE VOID SIZE DISTRIBUTION

5.3.1 The void size distribution of mono-disperse medium

For mono-disperse medium, the void size distribution shows only one peak (see by Figure 12), which implies the size of each void space is identical. AIC of normal model is -1971.67 and AIC of bi-normal model is -1921.56, which indicates normal model fits better. This result also shows that k=0 and β=0:

$$\frac{\Delta p}{L} = \frac{150 u \mu}{{D_p}^2 \varepsilon^3} \tag{5.3.1}$$

This equation is also known as the Kozeny-Carman equation. In short, there is no channel formed in mono-disperse medium during filtration, so the Kozeny-Carman equation can applied in this situation.

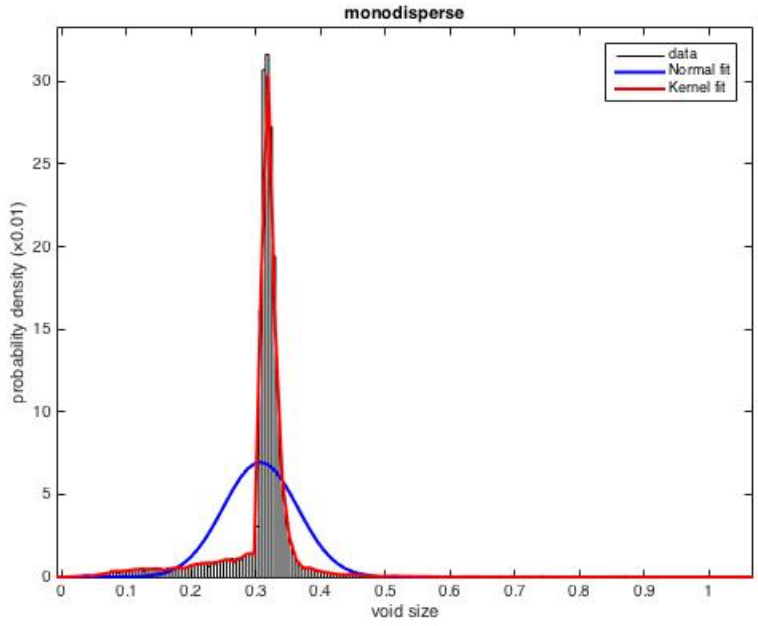

Figure 12. Probability density functions of the void size for mono-disperse system

5.3.2 The void size distribution of multi-disperse medium

For the multi-disperse medium, the void size distribution can be represented with several fit methods. In this thesis, Kernel distribution and Bi-normal (bimodal) distribution were chosen; a detailed comparison of these two methods is included in Appendix F. In Figure 13 (a), there are three sharp peaks in the Kernel distribution, which indicates that there are three void sizes in the cake: the largest one is the main void size, and the other two peaks are caused by the deformation of the cakes. For the simulation of binary mixing $R_{s/l}$=0.84, two size channels were formed during the experiments; therefore, the total void space is larger, causing an increase in the flow rate. AIC of normal model is -2767.57 and AIC of bi-normal model is -3516.19, which indicates bi-normal model fits better. By analysis with a much more common method: bi-normal distribution, two significant peaks are shown. From Figure 13 (b), two sharp peaks are evident in the Kernel distribution: for the simulation of binary mixing $R_{s/l}$=0.50, a big size channel formed, and the possibility to form this channel is quite large because a large probability density at that peak can be seen. Even though the difference between the two peaks in the Bi-normal distribution is not obvious (since the difference between two mean void sizes is small), the percentage of second peak is quite large as shown in Table 14. AIC of normal model is -2444.90 and AIC of bi-normal model is -3093.52, which indicates bi-normal model fits better. Hence, there is a significant impact on the bed's permeability. In short, in systems that include large size ratio mixing ($R_{s/l}$>0.50), particle packings are disordered such that they lead to channelling in the packed bed.

Similar to the experiment results, the void size distributions of binary mixing with small size ratios are quite similar to the mono-disperse void size distribution. From Figure 14 (a), even though two peaks are shown, these peaks are quite near to each other, which means the expanded

Table 14. Mean void sizes and the percentages of mixture of the second (expanded) normal for the void size bi-normal distribution of simulated beds

Size ratio ($R_{s/l}$)	Void size of first peak	Void size of second peak	Percentage of second peak
0.84	0.1707	0.2224	20.54%
0.50	0.1932	0.2199	45.86%
0.33	0.1820	0.2021	49.41%
0.20	0.2046	0.2154	31.43%

of void size is small and the deformation of the cake is very little. Also, AIC of normal model is -2554.70 and AIC of bi-normal model is -2510.21, which indicates normal model fits better. From Figure 14 (b), there are several small peaks with very low probability density, which also means the main structure is not changed. Also, AIC of normal model is -2643.16 and AIC of bi-normal model is -2578.67, which indicates normal model fits better.

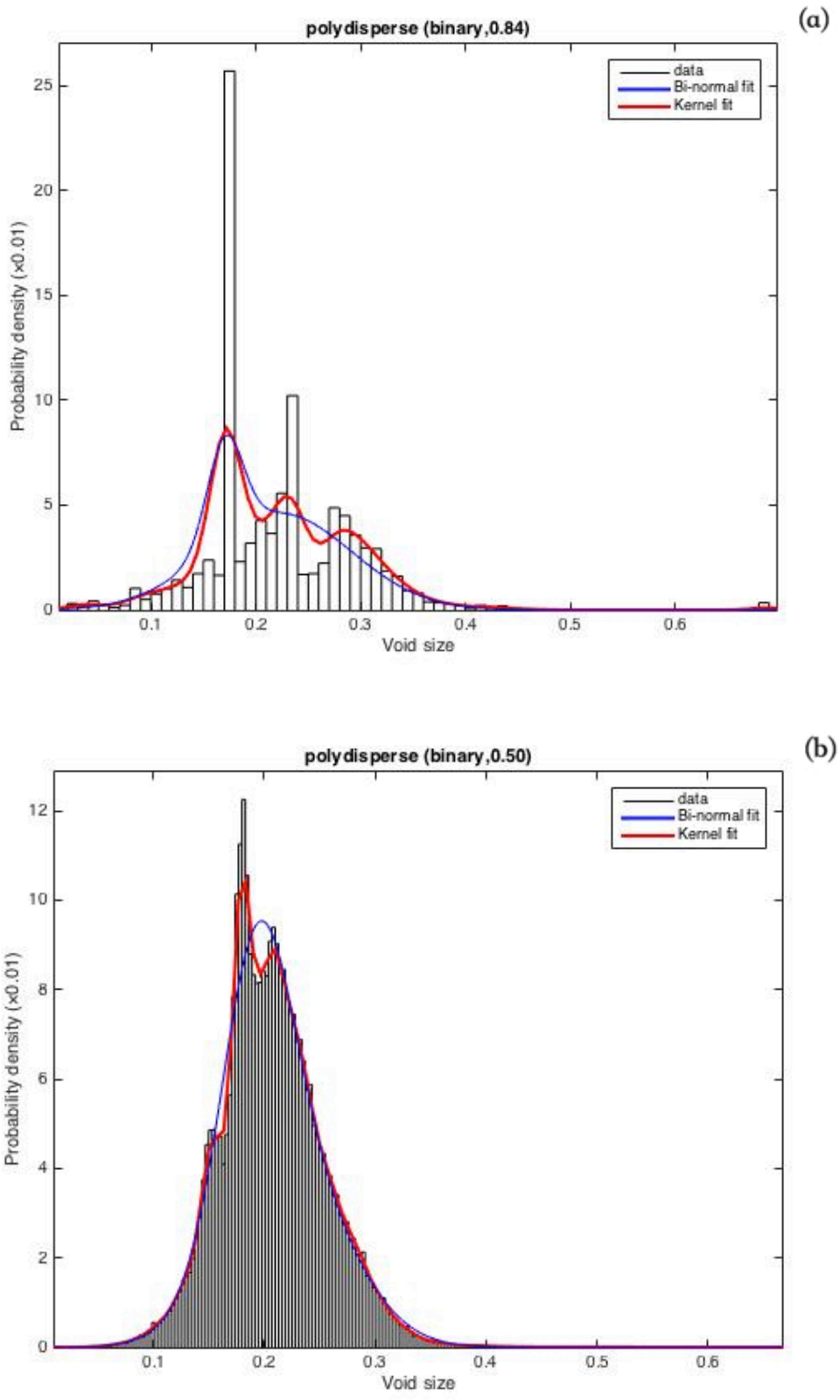

Figure 13. Probability density functions of the void size for multi-disperse system in large size ratio

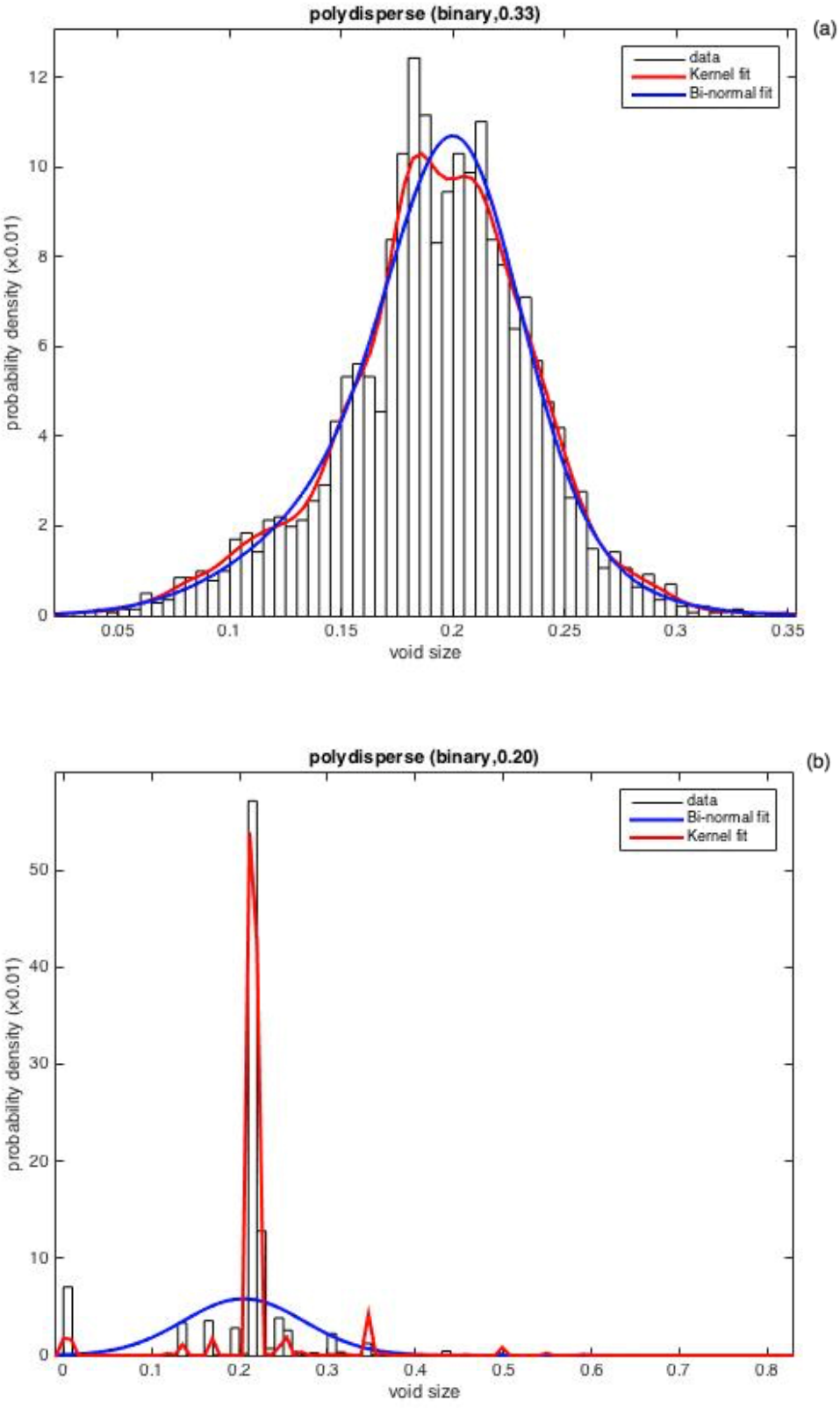

Figure 14. Probability density functions of the void size for multi-disperse system in small size ratio

5.4 APPLICATIONS OF MODIFIED EQUATION

In Chapter 5.1, a modified Kozeny-Carman equation is proposed based on theoretical derivation. To inspect the applicability of the modified equation we compare results using this model to empirical data. We should note that, in all cases, void model factors were measured by the Kernel distribution and the bi-normal distribution from DEM simulated results.

5.4.1 Application in binary mixing ($R_{s/l}$ =0.50)

Void factors determined by bi-normal distribution are based on different mean void sizes and probability density as shown in Table 14. The fraction of expanded voids is equal to the percentage of density of the second (expanded) peak (κ = 45.86%). The ratio of void sizes is equal to the ratio of two mean void sizes of two normal (β = 1.14). The error between the empirical flow rate and the predicted flow rate using the modified version of the Kozeny-Carman equation with void factors are 40.37%.

For Kernel distribution, we can get κ by calculating the number of occurrences at area B (the second peak) and the number of occurrence at the total area, as:

$$\kappa = \frac{number\ of\ occurence\ at\ area\ B}{number\ of\ total\ occurence} \times 100\% = 40.44\% \tag{5.4.1}$$

β is the expansion rate. It can be calculate by determining the mean void size of area B and the mean void size of a normal area A using:

$$\beta = \frac{mean\ void\ size\ of\ area\ B}{mean\ void\ size\ of\ normal\ area\ A} = 1.24 \tag{5.4.2}$$

We can calculate the predicted flow rate using the κ and β we calculated from the simulation of the void size distribution. The relationship between operating pressure and flow rate is shown in Figure 16. The error between empirical flow rate and predicted flow rate based on the Kozeny-

Carman equation is very large; the error between empirical flow rate and predicted flow rate based on the modified Kozeny-Carman equation in this thesis is much smaller (as shown in Table 15), just as we expected. Similarly, the goodness-of-fit statistics also illustrate fit models are more reliable to predict flow rate as value of R-Square (see by Table 15) are significantly increased.

Table 15. Comparing empirical results to model fits in binary disperse system ($R_{s.l}$=0.50)

Data	Error	SSE	R-square	RMSE
CK equation	110.85%	5.821e-09	0.7543	3.412e-05
Kernel fit	9.55%	6.119e-11	0.9974	3.498e-06
Bi-normal fit	40.37%	1.385e-09	0.9415	1.664e-05

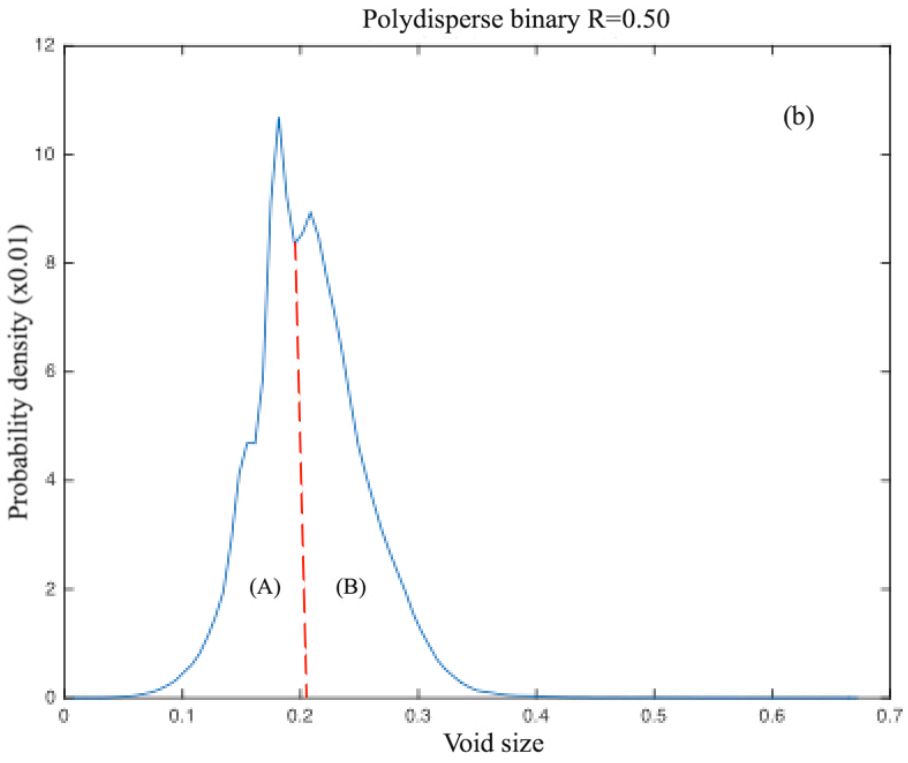

Figure 15. Analysis of the void size for Binary mixing: $R_{s/l}$=0.50

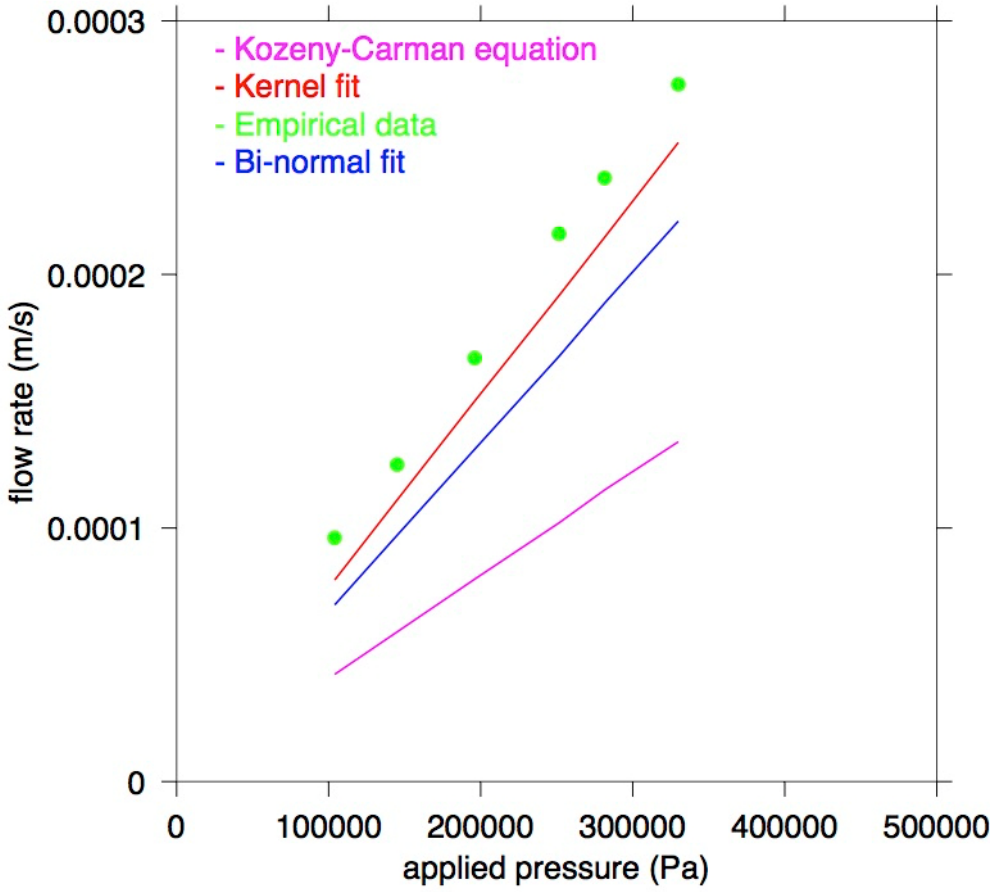

Figure 16. The relationship between operating pressure and flow rate of binary mixing $R_{s/l}$=0.50

5.4.2 Application in binary mixing ($R_{s/l}$ =0.84)

Method that used to determine the void factors by bi-normal distribution is similar to chapter 5.4. The fraction of expanded voids is equal to the percentage of density of the second (expanded) peak (κ = 20.54%). The ratio of void sizes is equal to the ratio of two mean void sizes of two normal (β = 1.30). The error between the empirical flow rate and the predicted flow rate using the modified version of the Kozeny-Carman equation with void factors are 25.68%.

For Kernel distribution, we can determine κ_1 and κ_2 by calculating the number of occurrence at area B and C with the number of occurrence at the total area from Figure 17, as:

$$\kappa_1 = \frac{\text{number of occurence at area B}}{\text{number of total occurence}} = 18.11\% \tag{5.4.3}$$

$$\kappa_2 = \frac{\text{number of occurence at area C}}{\text{number of total occurence}} = 7.87\% \tag{5.4.4}$$

β_1 and β_2 are calculate using the mean void size of area B and C, with the mean void size of a normal area A as determined by:

$$\beta_1 = \frac{\text{mean void size of area B}}{\text{mean void size of normal area A}} = 1.37 \tag{5.4.5}$$

$$\beta_2 = \frac{\text{mean void size of area C}}{\text{mean void size of normal area A}} = 1.78 \tag{5.4.6}$$

Using κ_1, κ_2 and β_1, β_2 in order to calculate the predicted flow rate we note the relationship between operating pressure and flow rate as shown in Figure 18. The error between empirical flow rate and predicted flow rate based on the Kozeny-Carman equation is quite large. Conversely, the error between the empirical flow rate and the predicted flow rate using the modified version of the Kozeny-Carman equation in this thesis is much smaller (as shown in Table 16), as we expected. Similarly, the value of R-Square is significantly increased with a modified model.

Table 16. Comparing empirical results to model fits in binary disperse system ($R_{s,l}$=0.84)

Data	Error	SSE	R-square	RMSE
CK equation	87.71%	6.128e-10	0.7803	1.107e-05
Kernel fit	-23.07%	6.119e-11	0.9775	3.54e-06
Bi-normal fit	25.68%	1.385e-09	0.9557	4.972e-06

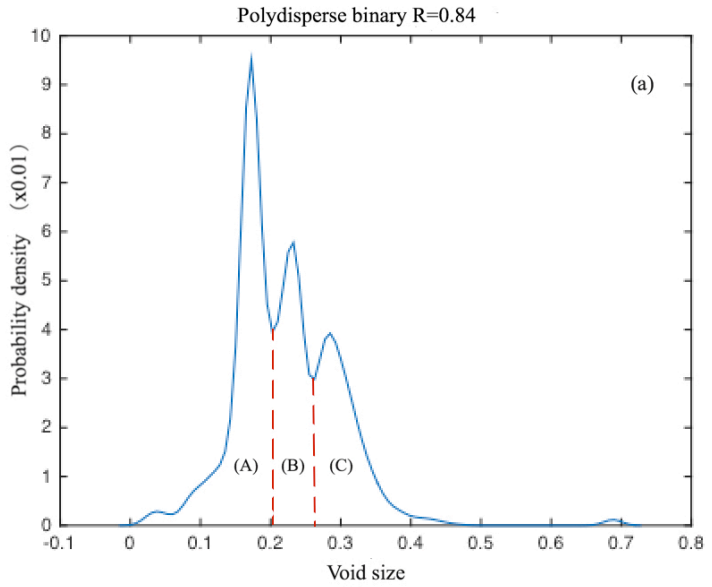

Figure 17. Analysis of the void size for Binary mixing: $R_{s/l}$=0.84.

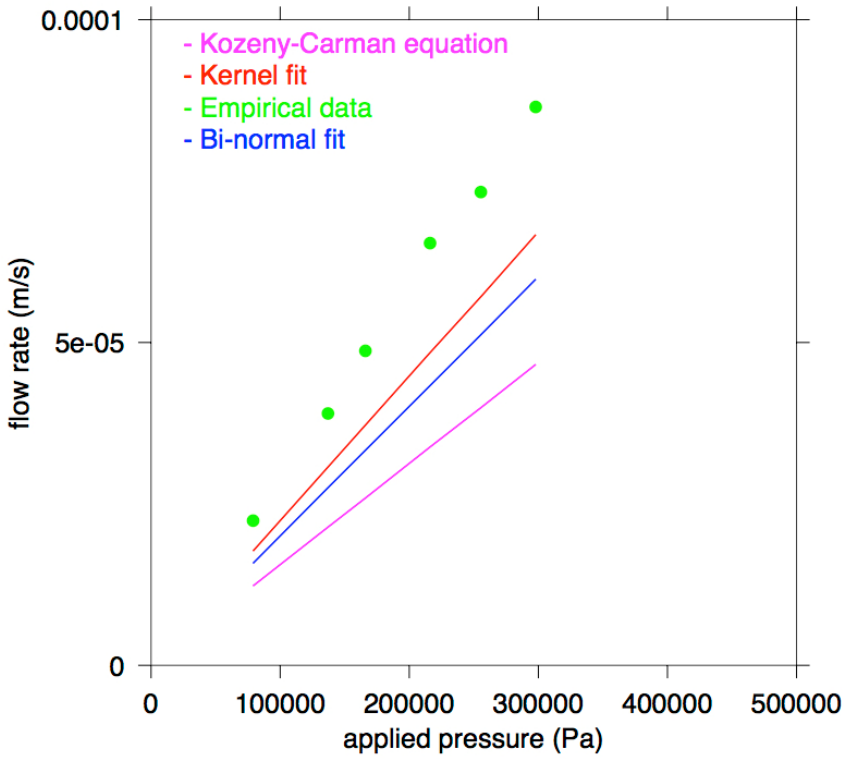

Figure 18. The relationship between operating pressure and flow rate of binary mixing $R_{s/}$=0.84.

As shown above, if the void size distribution for a specify cake is known, we can determine the fraction of expanded voids and the ratio of void sizes, then the predicted flow rate can be calculated with the modified Kozeny-Carman equation at a certain ultimate pressure drop.

6.0 CONCLUSION

By comparing experimental results to those predicted from the Kozeny-Carman model/equation, we assess the utility of this equation for application to systems that include poly-disperse particles at moderate fluid pressure. We find substantial agreement between model and experiment only for systems that result in well-ordered particle packing. Dramatic disagreement is observed for particle beds that exhibit wide void size distributions, as these particles cannot form order packings. We hypothesized and the tested that these disordered packings lead to channeling which ultimately causes more fluid to flow through the cake. In contrast, cakes that are composed of mono-disperse particles form ordered packings that lead to a tight void size distribution. Additionally, cake structures can be quite complicated in multi-disperse systems. For multi-disperse cakes, if the size range of particles is quite small, then particles can be treat as uniform in size for equation purposes. However, when the size range of particles is large (>10% difference), the cake structure is quite different from a mono-disperse one, where the Kozeny-Carman equation is not suitable to predict the flow behavior.

As the structure of a cake that is composed of multi-disperse particles can be very complicated, we focused on representing cake structures in binary systems. As discussed in Chapter 3.0 , particles with $R_{s/l}<0.5$ can be packed efficiently, and particles with $R_{s/l}>0.5$ cannot be packed in order. The experiment results, which are shown in chapters 2.0 and 3.0, show that the changes in fluid properties are based on the differences of structure of cakes in different size

ratios. Based on the Delaunay Tesselation method, we extract the void size distributions of simulated beds that are modeled by DEM simulation and comprised of the same size ratios used in the experiments. The void structures are represented by the probability density functions of pore sizes. Therefore by analyzing the void size distribution fitted by bi-normal distribution and Kernel distribution, the fraction of expanded voids (κ) and the ratio of void sizes (β) can be calculated as shown in Chapter 5.0 . A modified Kozeny Carman equation is presented in Chapter 5.1. The predicted flow dynamics from the equation with factors κ and β extracted from the simulation results are found to be much more similar to the experimental flow rates than those calculated using the unmodified Kozeny-Carman equation. In short, the effect of the void size distribution on filtration cakes is important. For a multi-disperse system, the prediction of flow rate should also consider the percentage of disordered particles and the expanded rate during the filtration. The modified equation is deemed reliable at predicting the flow behavior, provided that an accurate representation of the void size distribution is available.

6.1 FUTURE WORK

The next step for this project is trying to figure out the real void size distributions. The expansion factors we added to the modified the Kozeny-Carman are based on the representation of the void size distribution of the simulated beds, the difference between the simulated beds and the filtration cakes of the experiments are indeterminate. Furthermore this representation is based on the Delaunay tessellation, which may lead to inaccurate identification of pore locations and sizes because it may subdivide a pore into too many void spaces [39]. Even though a more reasonable

void size distribution can be achieved by merging Delaunay cells [40], it is very difficult to identify which tetrahedral should be merged. Thus, detailed analysis to achieve a more accurate void size distribution should be explored in the future. In this thesis, we focused on the void size distribution of layer-by-layer beds. Analyses for random packed bed are not very well as shown in Appendix C. Further work should explore how to provide an approximate representation of the void size distribution of a random packed bed during a filtration process.

Because the void size distribution changes in different situations, it is difficult to get a certain modified equation with a certain distribution-fitting model. In further work, the relative quality of different models based on the assumptions of different numbers of expanded rates can be measured based on the Akaike information criterion so that a demarcation point of size ratio can be explored in order to divide models into applications for different situations.

Particle interactions are a major part of filtration; in this thesis the main point is trying to figure out the relationship between fluid properties and cake structure during a filtration process. The relationship between flow properties and individual pore geometry should be further explored. Therefore, the Lattice Boltzmann Method (LBM) simulation is needed to mimic fluid dynamics. LBM is a computational model that is widely used in designing models of the physics properties of fluid flow as we shortly introduced in Chapter 1.4.2.

In this thesis, simple spherical glass beads were chosen to compose the filtration cake. However, particles that are used in real industries are almost never spherical. So it is essential to analyze the complexity of particles. This means that particle shapes should be considered when try to determine the cake structure and flow rate during filtration. Adding impurity into a filter should also be studied in the future.

APPENDIX A

MODEL OF PARTICLE PLACES IN DIFFERENT SIZE RATIO

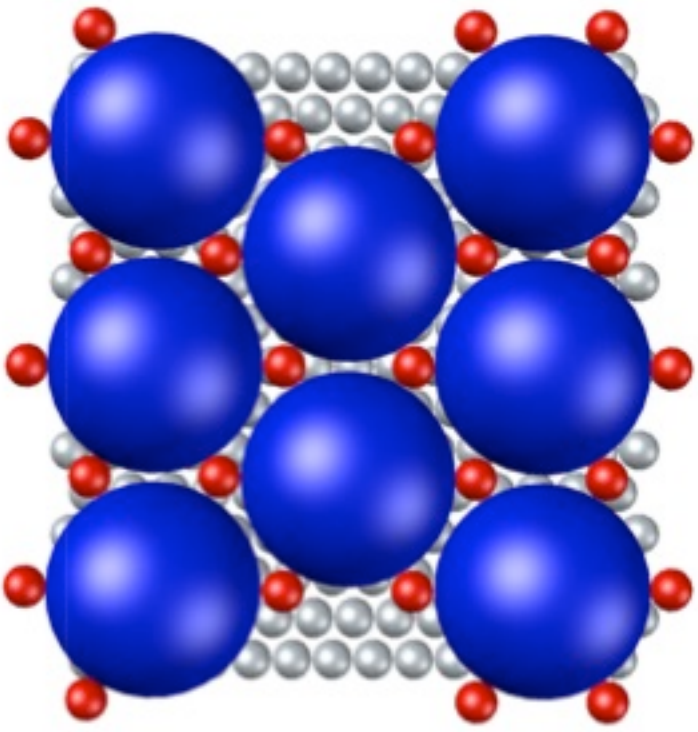

Figure 19. Model of binary mixing particles ($R_{s/l}$=0.20) based on Ref. [22]

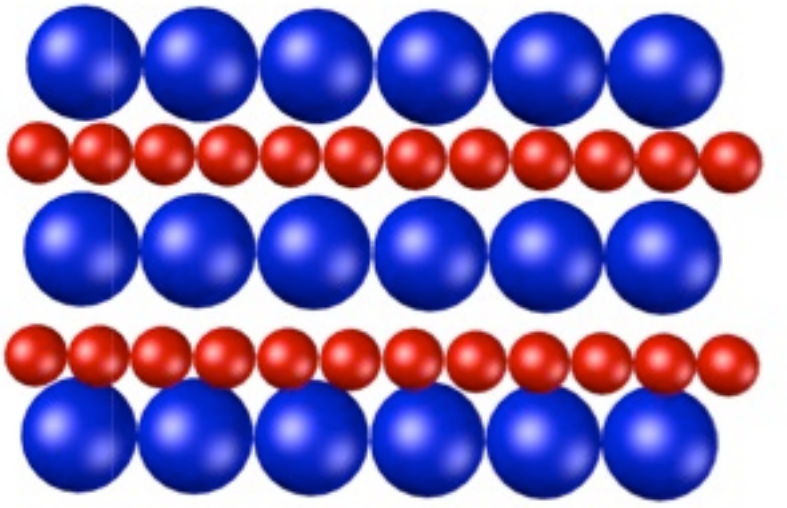

Figure 20. Model of binary mixing particles ($R_{s/l}$=0.50) based on Ref. [22]

APPENDIX B

FIGURES OF SIMULATED BEDS BY DEM METHOD

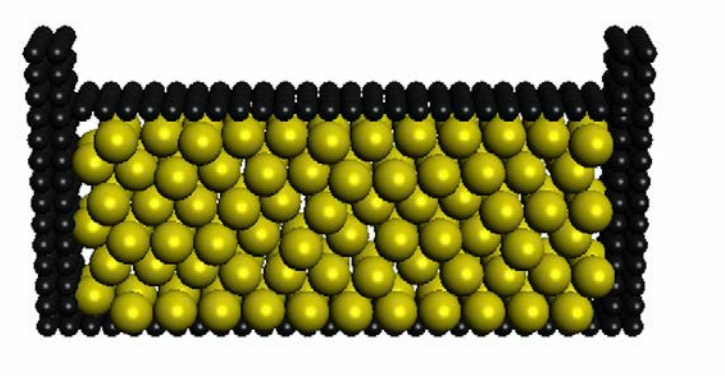

Figure 21. Simulated bed of mono-disperse system

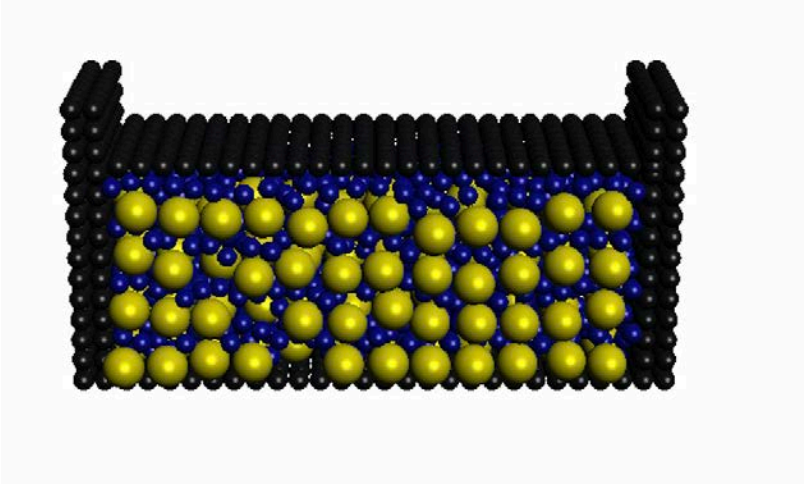

Figure 22. Simulated bed of binary-disperse system

APPENDIX C

ANAYLYSIS OF SIMULATIONS OF RANDOM PACKED BEDS

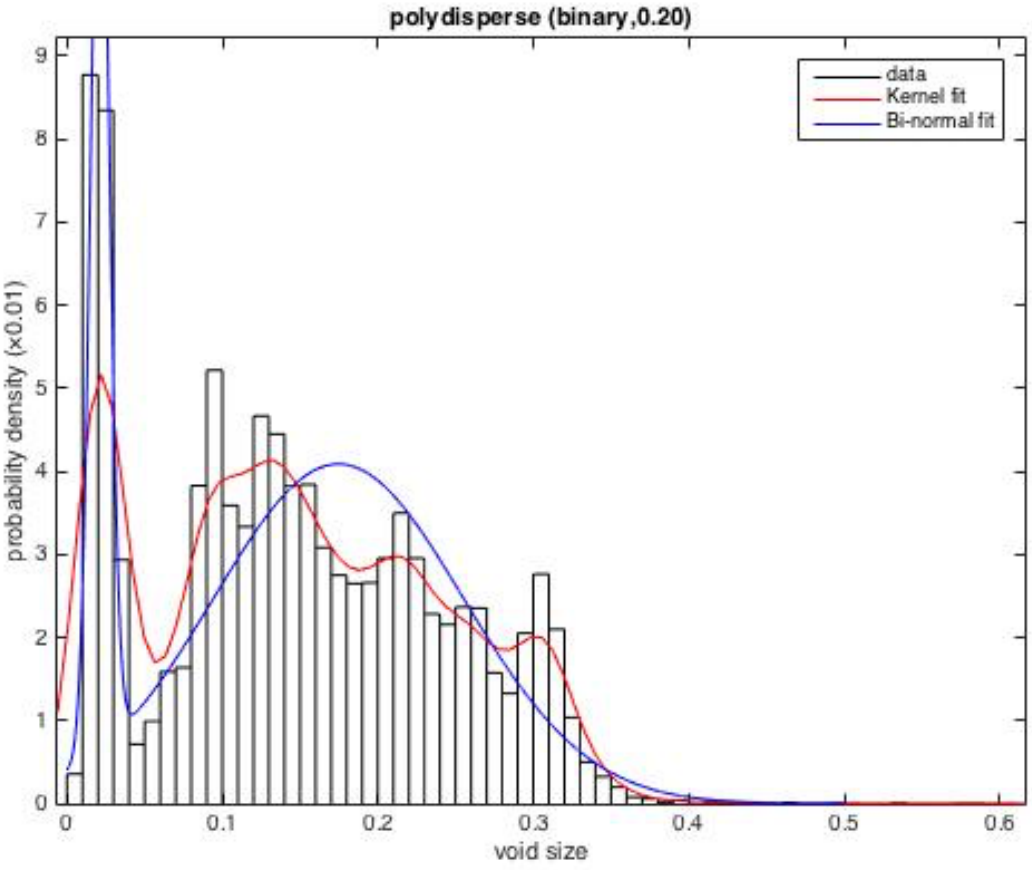

Figure 23. Probability density functions of the void size in Binary distribution ($R_{s/l}$ = 0.20)

As we simulated packed beds layer-by-layer in Chapter 4.0 , other beds were simulated based on random packing. Figure 23 shows the void size distribution in binary system ($R_{s/l}$ =0.20), an obviously peak can be found at a very small void size, which indicates most of small particles are settled in the bottom of the bed. These small particles influence the void size distribution as several small peaks can be seen in Figure 23. Figure 24 also shows a peak at small void size. The results predicted by this void size distribution are much larger than the empirical results as the simulated bed is deformed. As shown in Table 17, the value of R-square decreases much with the fit of simulation data of random packed bed.

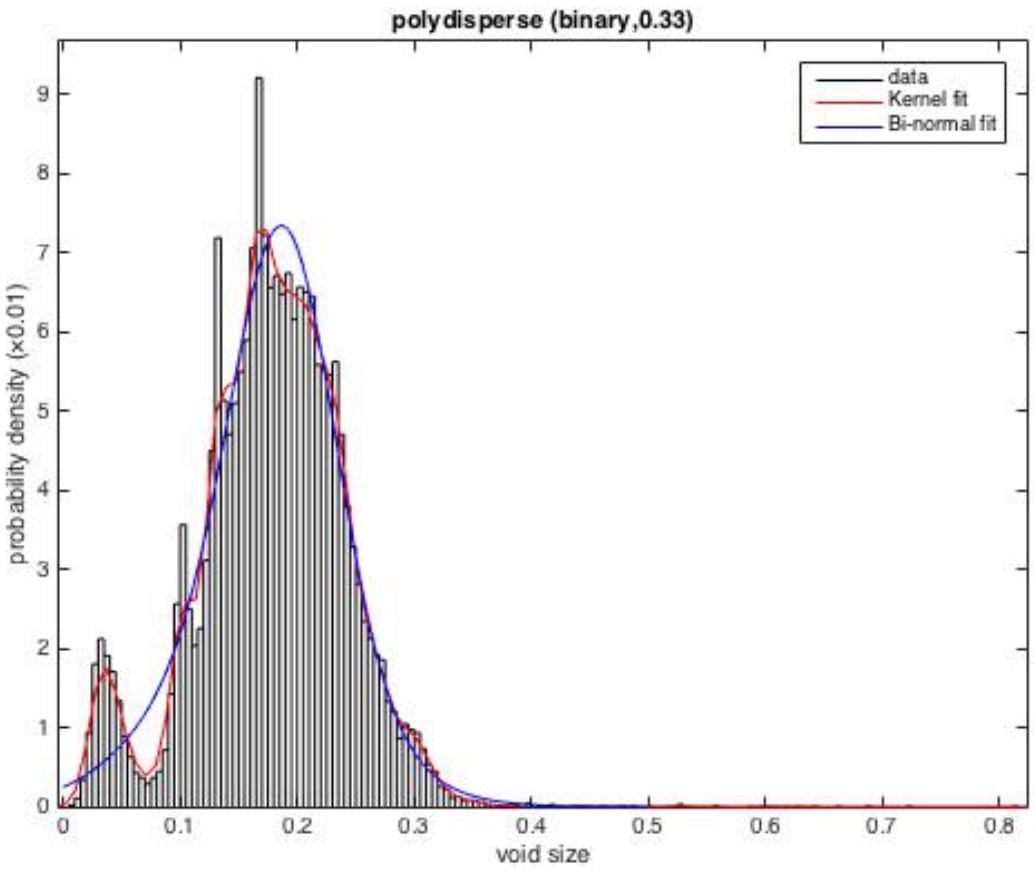

Figure 24. Probability density functions of the void size in Binary distribution ($R_{s/l}$ = 0.33)

Table 17. Comparing empirical results to model fits in binary disperse system ($R_{s.l}$=0.33)

Data	Error	SSE	R-square	RMSE
CK equation	11.17%	1.957e-09	0.9901	1.978e-05
Bi-normal fit	-21.97%	5.799e-08	0.7073	1.077e-04

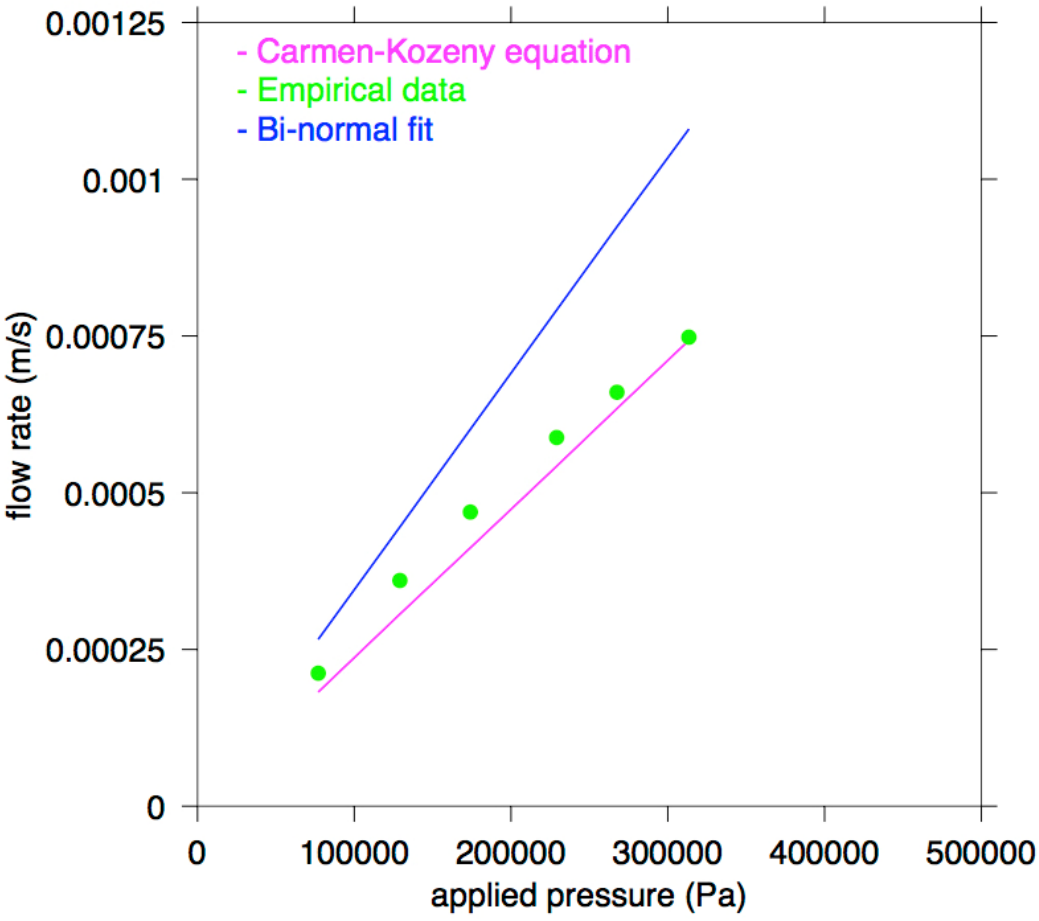

Figure 25. The relationship between operating pressure and flow rate of binary mixing $R_{s/}$=0.33

Figure 26 shows two nearby peaks. The results predicted by this void size distribution are better than the results predicted by Kozeny-Carman equation (see by Figure 27). However, as shown in Table 18, the value of R-square is little smaller than the value based on layer-by-layer simulation. Thus, the flow rate is unpredictable with the simulation analysis of a random packed bed. Further work should explore how to provide an approximate representation of the void size distribution of a random packed bed to predict the flow behavior.

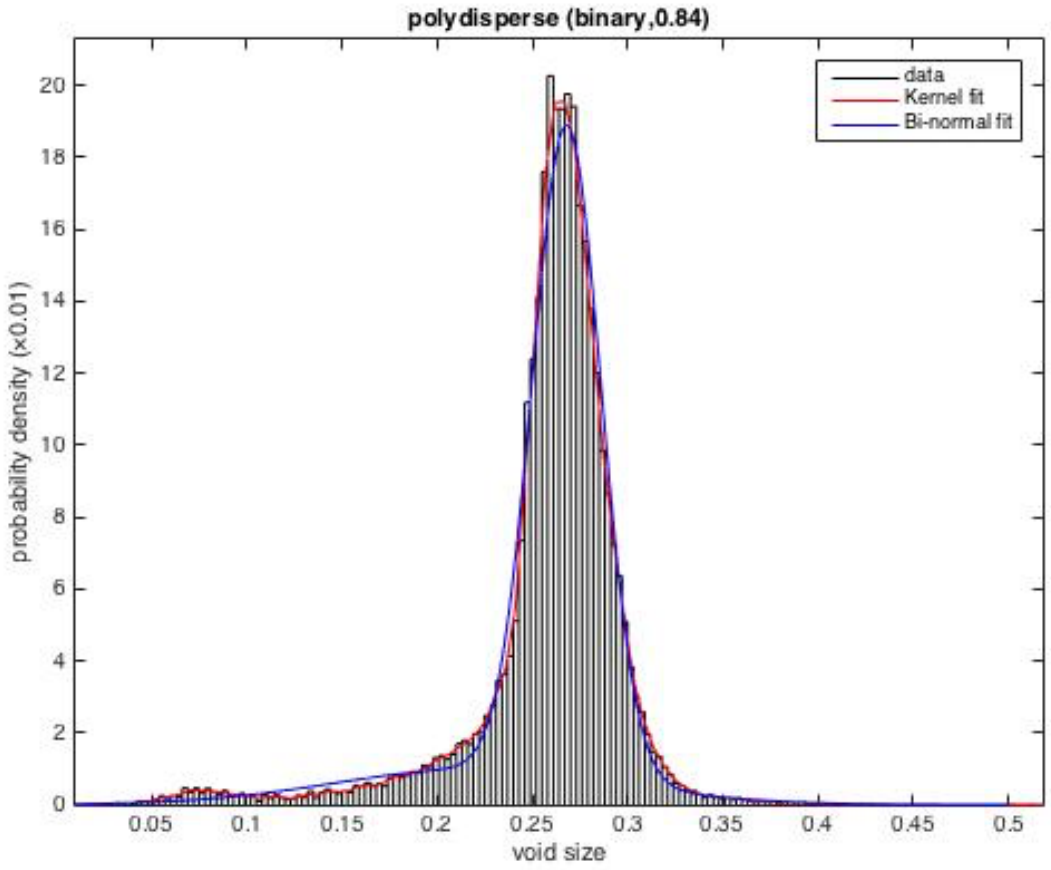

Figure 26. Probability density functions of the void size in Binary distribution ($R_{s/l}$ = 0.84)

Table 18. Comparing empirical results to model fits in binary disribution ($R_{s.l}$=0.84)

Data	Error	SSE	R-square	RMSE
CK equation	87.71%	6.128e-10	0.7803	1.107e-05
Bi-normal fit	43.71%	2.660e-10	0.9046	7.293e-06

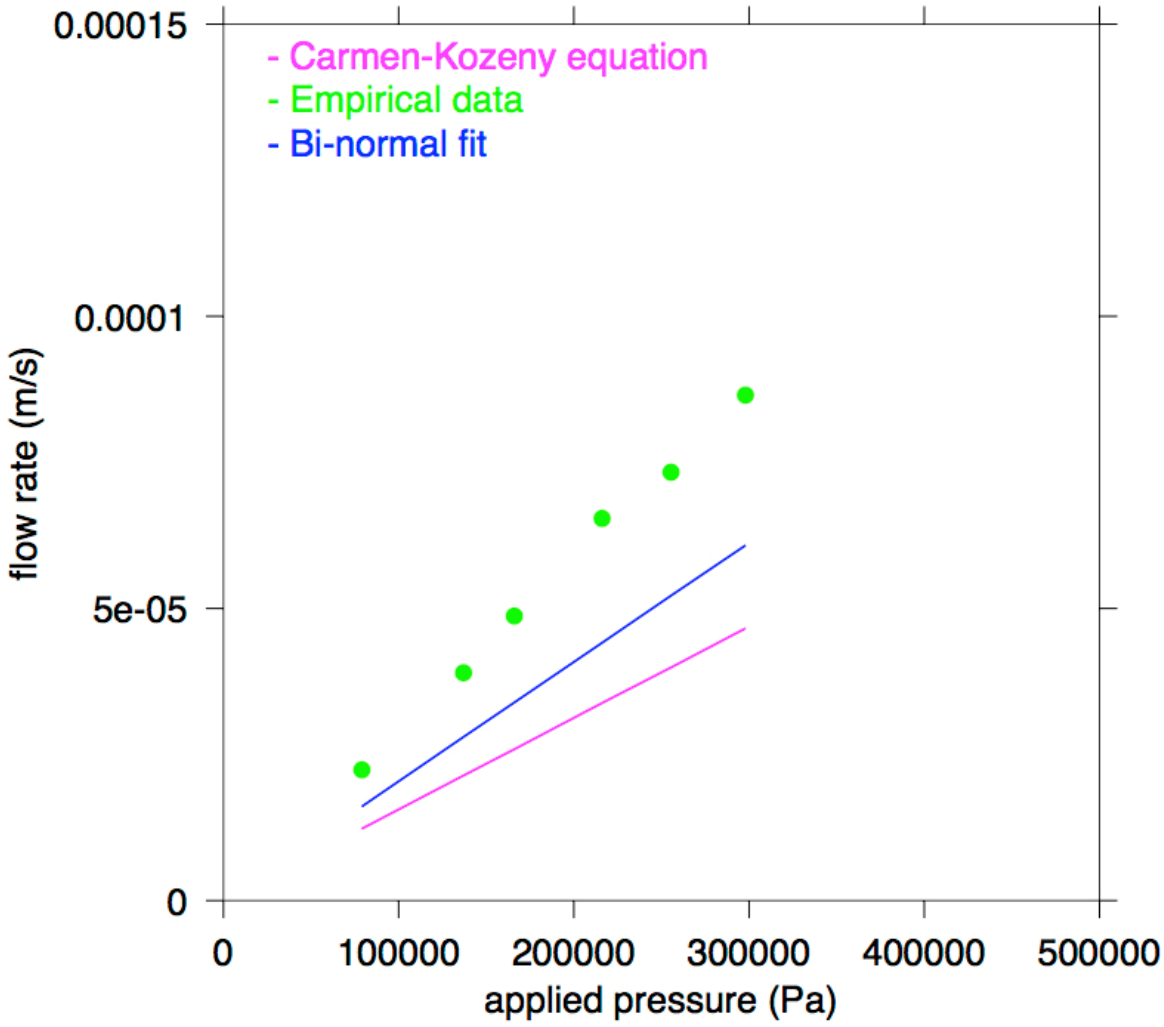

Figure 27. The relationship between operating pressure and flow rate of binary mixing $R_{s/}$=0.84

APPENDIX D

SUPPOSE OF THE MODIFED KOZENY-CARMAN EQUATION

In traditional theoretical approach (Kozeny-Carman equation), pores in the cake are replaced by circular channels, maintaining the same surface area and void volume as shown in Figure 28. And a superficial velocity is assumed to be constant in all pores.

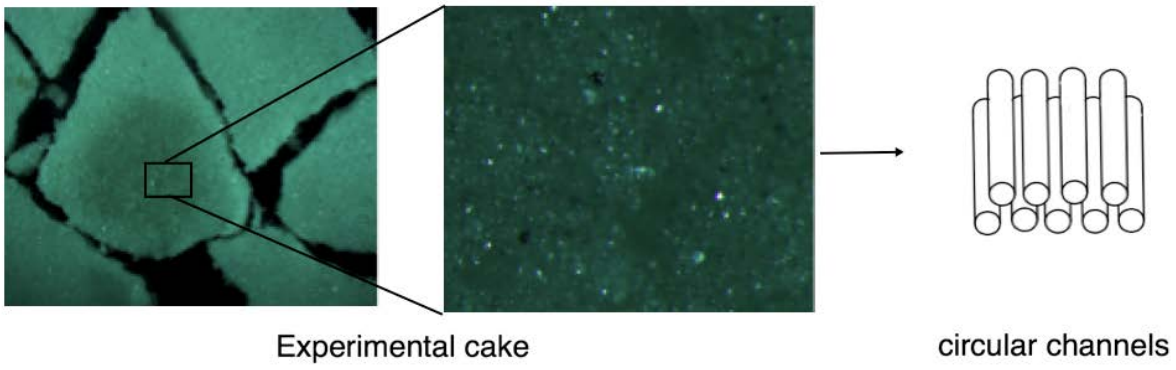

Figure 28. Replace pores with circular channels (match S_a and εV)

The tortuosity factor λ is added to capture bends to increases superficial velocity linearly. The tortuosity is the length of the actual flow path divided by the linear distance between the ends of

the flow path as shown in Figure 29. To modified the Kozeny-Carman equation, we assumed the increase of flow rate in multi-disperse system is caused by the deform of the cake structure, which means the void tubes (circular channels) are enlarged as shown in Figure 30.

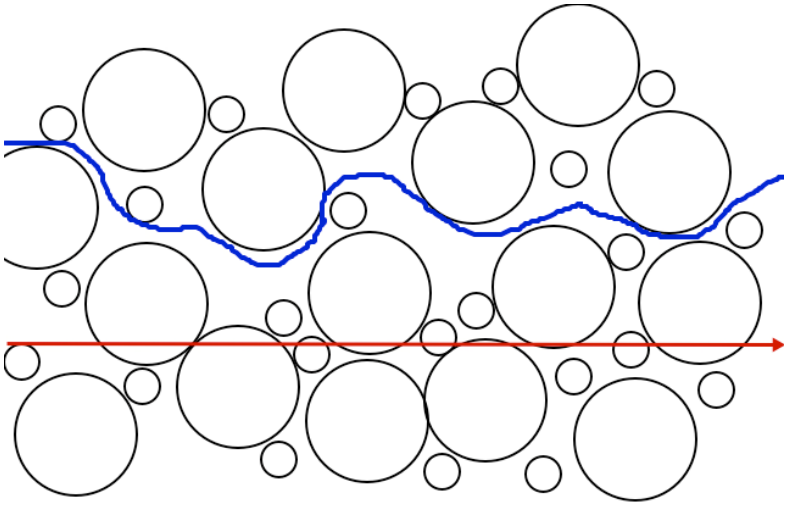

Figure 29. Tortuosity (red line: straight-line distance; blue line: a potential flow path)

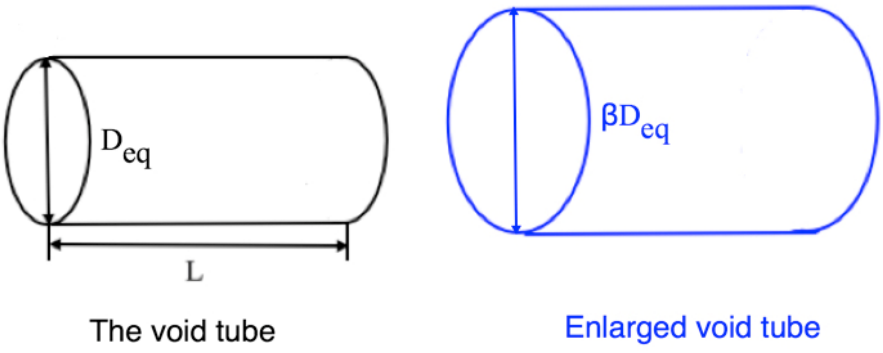

Figure 30. Diameter of the void tube is enlarged β during the filtration process in multi-disperse system

APPENDIX E

MATLAB CODE FOR REPRESENT THE VOID SIZE DISTRIBUTION

```
%%Kernel distribution%%
A=load('0.75_1kPa.txt');
x=A(:,1);
y=A(:,2);
z=A(:,3);
T = delaunayTriangulation(x,y,z);
coords=[x,y,z];
V=zeros(size(T,1),1);
R=zeros(size(T,1),1);
for i=1:size(T,1)
V(i) = 1/6*abs(dot(coords(T(i,2),:)-coords(T(i,1),:),cross(coords(T(i,3),:)-
coords(T(i,1),:),coords(T(i,4),:)-coords(T(i,1),:))));
R(i) = (V(i)./pi/4*3).^(1/3);
end
[f,xi]=ksdensity(R);
hist(R,0:.00001:0.5);
plot(xi,f)
```

```
title('Polydisperse binary  R = 0.20')

legend('Kernel Distribution')

xlabel('void size');ylabel('Probability density');


%%Bi-normal distribution%%

A1=load('0.326');

x1=A1(:,1);

y1=A1(:,2);

z1=A1(:,3);

T1 = delaunayTriangulation(x1,y1,z1);

coords=[x1,y1,z1];

V1=zeros(size(T1,1),1);

R1=zeros(size(T1,1),1);

for i=1:size(T1,1)

V1(i) = 1/6*abs(dot(coords(T1(i,2),:)-coords(T1(i,1),:),cross(coords(T1(i,3),:)-

coords(T1(i,1),:),coords(T1(i,4),:)-coords(T1(i,1),:))));

R1(i) = (V1(i)./pi/4*3).^(1/3);

end

x = R1;

pdf_normmixture = @(x,p,mu1,mu2,sigma1,sigma2) ...

                    (1-p)*normpdf(x,mu1,sigma1) + p*normpdf(x,mu2,sigma2);

pStart = .5;

muStart = quantile(x,[0.25 0.75])
```

```
sigmaStart = sqrt(var(x) - .25*diff(muStart).^2)

start = [pStart muStart sigmaStart sigmaStart];

lb = [0 -Inf -Inf 0 0];

ub = [1 Inf Inf Inf Inf];

paramEsts = mle(x, 'pdf',pdf_normmixture, 'start',start, 'lower',lb, 'upper',ub)

statset('mlecustom')

options = statset('MaxIter',1000, 'MaxFunEvals',2000);

paramEsts = mle(x, 'pdf',pdf_normmixture, 'start',start,'lower',lb, 'upper',ub, 'options',options)

x=0:0.00001:0.5;

sigma1=0.007302;

y = pdf_normmixture(x,paramEsts(1),paramEsts(2),paramEsts(3),paramEsts(4),paramEsts(5));

plot(x,y,'-b')

legend('Bi-normal distribution');

xlabel('void size');

ylabel('Probability density (×0.01)');
```

APPENDIX F

COMPARE THE KERNEL DISTRIBUTION WITH THE BI-NOMRAL DISTRIBUTION

The chi-square test determines if data fit a specified probability distribution, with parameters estimated from the data [41]. It returns a test decision for the null hypothesis that the data in vector x comes from a normal distribution with a mean and variance estimated from x:

$$\chi^2 = \sum_{i=1}^{N} (O_i - E_i)^2 / E_i$$

where O_i are the observed counts and E_i are the expected counts based on the hypothesized distribution. For Kernel distribution in this thesis, h=1, p=1.5387e-57. For Bi-normal distribution in this thesis, h=1, p=0.

h=1 indicates that chi2gof rejects the null hypothesis at the default 5% significance level[41], which means this two distribution models are not quite fit with the data. p is the probability of observing a test statistic as excessive as, the observed value under the null hypothesis, and a smaller value of p cast doubt on the validity of the null hypothesis [41], which also means Kernel distribution is more similar with the collected data.

Kolmogorov-Smirnov test can compare these two distributions with the factor k: k is the quantified distance between the data and the distribution [41]. A lower k value signifies a better agreement between the distribution and the data. k of Kernel is 0.0187 ,which is much smaller than the Bi-normal one (0.3085). Kernel distribution is more reliable as it fit every data very well. However, Kernel distribution is a non-parametric one, which means it is really hard to get

parameters. Bi-normal distribution can achieve parameters (like mean size) directly that makes calculation more convenient.

APPENDIX G

PARITY PLOTS (COMPARE EMPIRICIAL RESULTS WITH PREDICTED DATA)

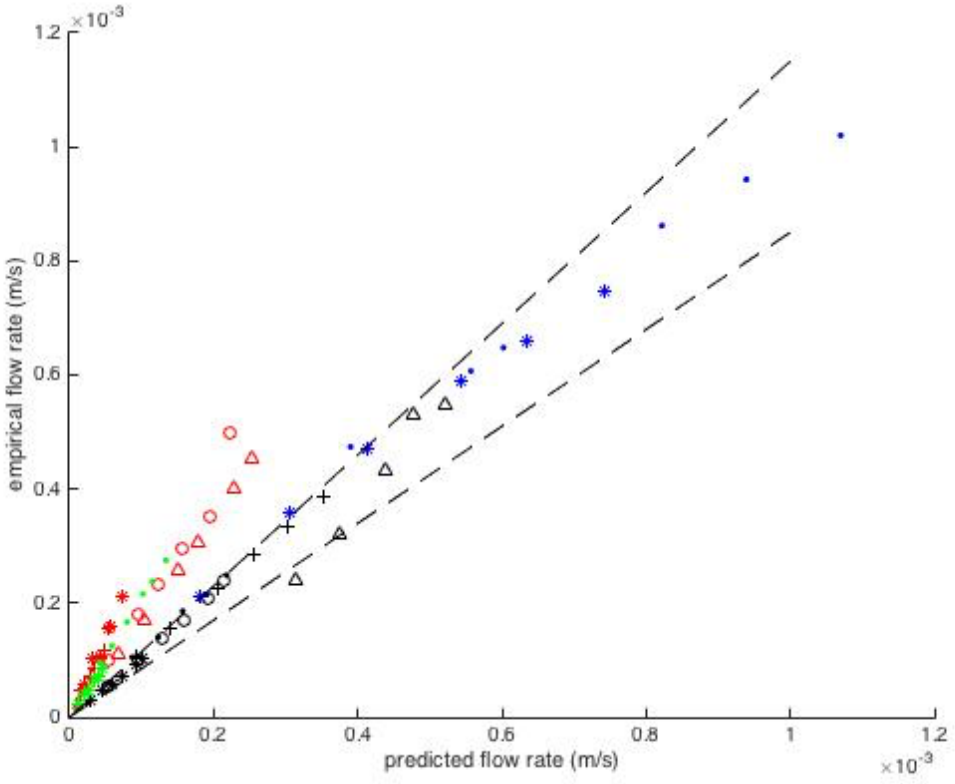

Figure 31. Empirical vs Predicted flow rate (narrow size distribution: •, 53-63µm; +, 63-75µm; *, 75-90µm; o, 90-106µm; △, 500µm; wide size distribution: •, 50-75µm; +, 50-100µm; *, 75-100µm; o, 150-177µm; △, 180-210µm; Binary distribution: •, $R_{s/l}$=0.5; *, $R_{s/l}$=0.84; •, $R_{s/l}$=0.2; *, $R_{s/l}$=0.33; and --, ± 15% error)

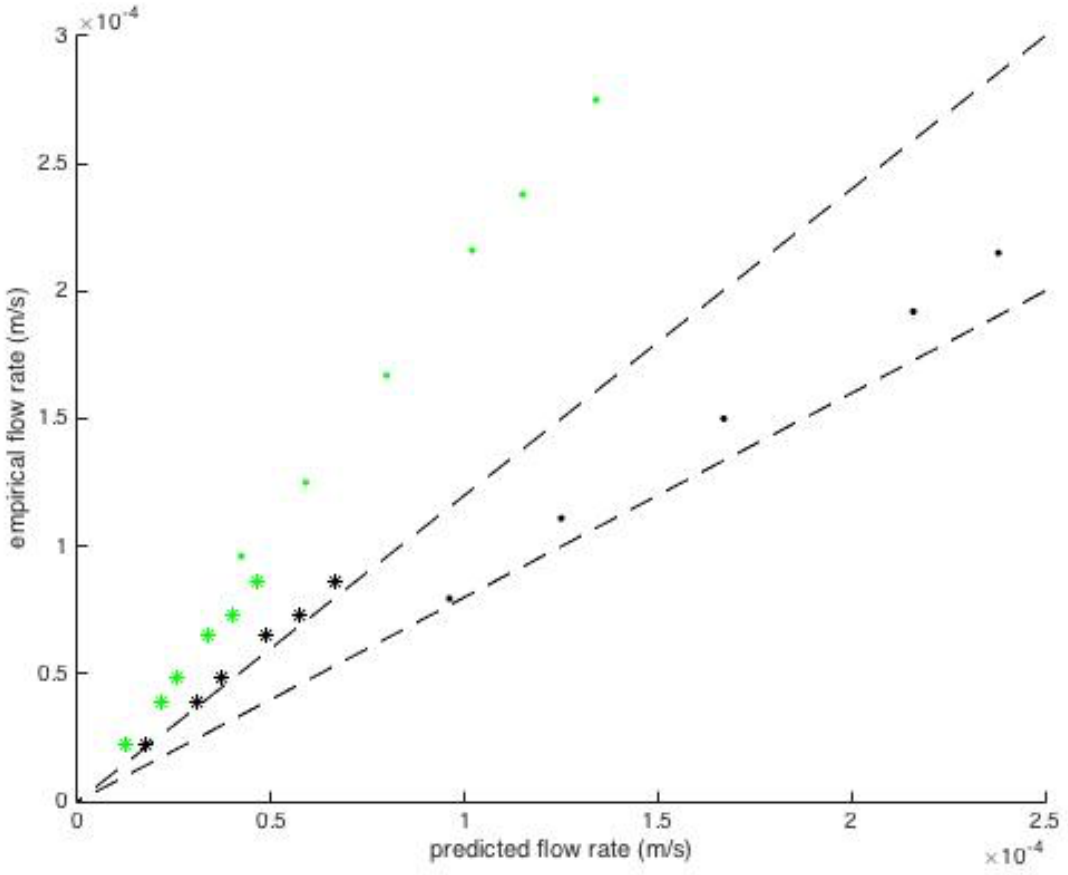

Figure 32. Empirical vs Predicted flow rate (Predicted by Kozeny-Carman equaiton: •, $R_{s/l}$=0.5; *, $R_{s/l}$=0.84; Predicted by modified equation •, $R_{s/l}$=0.5; *, $R_{s/l}$=0.84; and --, ± 15% error)

BIBLIOGRAPHY

[1]. Tien, Chi. Introduction to cake filtration: analyses, experiments and applications. Elsevier, 2006.

[2]. Abboud, Nelly M., and M. Yavuz Corapcioglu. "Modeling of compressible cake filtration." Journal of colloid and interface science 160, no. 2 (1993): 304-316.

[3]. Nield, Donald A., and Adrian Bejan. Mechanics of Fluid Flow Through a Porous Medium. Springer New York, 2013.

[4]. Kavoosi, Azad. "Investigating the Fundamental Parameters of Cake Filtration using a Gravity Column Device." PhD diss., 2014.

[5]. Rushton, Albert, Anthony S. Ward, and Richard G. Holdich. Solid-liquid filtration and separation technology. John Wiley & Sons, 2008.

[6]. Ruth, B. F. "Correlating filtration theory with industrial practice." Industrial & Engineering Chemistry 38, no. 6 (1946): 564-571.

[7]. Grace, H. P. "Resistance and compressibility of filter cakes." Chemical Engineering Progress 49, no. 6 (1953): 303-318.

[8]. Tiller, F. M. "The role of porosity in filtration part 3: Variable- pressure—variable- rate filtration." AIChE Journal 4, no. 2 (1958): 170-174.

[9]. Shirato, M., and S. Okamura. "Behaviours of gaisome-clay slurries at constant pressure filtration." Kagaku Kagaku 20 (1956): 678-684.

[10]. Shirato, Mompei, Masao Sambuichi, Hiroo Kato, and Tsutomu Aragaki. "Internal flow mechanism in filter cakes." AIChE Journal 15, no. 3 (1969): 405-409.

[11]. Carman, Philip Crosbie. Flow of gases through porous media. Academic press, 1956.

[12]. Mauran, S., L. Rigaud, and O. Coudevylle. "Application of the Carman–Kozeny Correlation to a High- Porosity and Anisotropic Consolidated Medium: The Compressed Expanded Natural Graphite." Transport in Porous Media 43, no. 2 (2001): 355-376.

[13]. Rong, L. W., K. J. Dong, and A. B. Yu. "Lattice-Boltzmann simulation of fluid flow through packed beds of spheres: Effect of particle size distribution."Chemical Engineering Science 116 (2014): 508-523.

[14]. Koch, Donald L., and Reghan J. Hill. "Inertial effects in suspension and porous-media flows." Annual Review of Fluid Mechanics 33, no. 1 (2001): 619-647.

[15]. Hoef, MA Van Der, R. Beetstra, and J. A. M. Kuipers. "Lattice-Boltzmann simulations of low-Reynolds-number flow past mono-and bidisperse arrays of spheres: results for the permeability and drag force." Journal of fluid mechanics528 (2005): 233-254.

[16]. Yin, Xiaolong, and Sankaran Sundaresan. "Fluid- particle drag in low- Reynolds- number polydisperse gas–solid suspensions." AIChE journal 55, no. 6 (2009): 1352-1368.

[17]. Cundall, Peter A., and Otto DL Strack. "A discrete numerical model for granular assemblies." Geotechnique 29, no. 1 (1979): 47-65.

[18]. Munjiza, A., T. Bangash, and N. W. M. John. "The combined finite–discrete element method for structural failure and collapse." Engineering fracture mechanics 71, no. 4 (2004): 469-483.

[19]. Mohamad, Abdulmajeed A. Lattice Boltzmann method: fundamentals and engineering applications with computer codes. Springer Science & Business Media, 2011.

[20]. Herdan, G. "Relation of the Harmonic Mean Particle Size to the Specific Surface of Participate Matter." (1950): 858-859.

[21]. Li, Liangxing, and Weimin Ma. "Experimental characterization of the effective particle diameter of a particulate bed packed with multi-diameter spheres."Nuclear Engineering and Design 241, no. 5 (2011): 1736-1745.

[22]. Lash, Melissa H., Jahnelle C. Jordan, Laura C. Blevins, Morgan V. Fedorchak, Steven R. Little, and Joseph J. McCarthy. "Non- Brownian Particle- Based Materials with Microscale and Nanoscale Hierarchy." Angewandte Chemie 127, no. 20 (2015): 5952-5956.

[23]. Gong, Guobin. "DEM simulations of drained and undrained behaviour." (2008).

[24]. Cundall, Peter A., and Otto DL Strack. "A discrete numerical model for granular assemblies." Geotechnique 29, no. 1 (1979): 47-65.

[25]. Johnson, Kenneth Langstreth, and Kenneth Langstreth Johnson. Contact mechanics. Cambridge university press, 1987.

[26]. Dong, K. J., R. P. Zou, R. Y. Yang, A. B. Yu, and G. Roach. "DEM simulation of cake formation in sedimentation and filtration." Minerals Engineering 22, no. 11 (2009): 921-930.

[27]. Eichholz, Christian, Hermann Nirschl, Fei Chen, and T. Alan Hatton. "DEM- simulation of the magnetic field enhanced cake filtration." AIChE Journal 58, no. 12 (2012): 3633-3644.

[28]. Hamaker, H. C. "The London—van der Waals attraction between spherical particles." physica 4, no. 10 (1937): 1058-1072.

[29]. Chu, K. W., and A. B. Yu. "Numerical simulation of complex particle–fluid flows." Powder Technology 179, no. 3 (2008): 104-114.

[30]. Aurenhammer, Franz. "Voronoi diagrams—a survey of a fundamental geometric data structure." ACM Computing Surveys (CSUR) 23, no. 3 (1991): 345-405.

[31]. Guibas, Leonidas J., Donald E. Knuth, and Micha Sharir. "Randomized incremental construction of Delaunay and Voronoi diagrams." Algorithmica 7, no. 1-6 (1992): 381-413.

[32]. Oger, L., J. P. Troadec, P. Richard, A. Gervois, and N. Rivier. "Voronoï tessellation of packings of equal spheres." Powders and grains 97 (1997): 287-290.

[33]. Richard, Patrick, Luc Oger, Jacques Lemaître, Liliane Samson, and Nikolai N. Medvedev. "Application of the Voronoï tessellation to study transport and segregation of grains inside 2D and 3D packings of spheres." Granular Matter1, no. 4 (1999): 203-211.

[34]. Yang, R. Y., R. P. Zou, and A. B. Yu. "Voronoi tessellation of the packing of fine uniform spheres." Physical Review E 65, no. 4 (2002): 041302.

[35]. Balhoff, Matthew T., and Karsten E. Thompson. "Modeling the steady flow of yield- stress fluids in packed beds." AIChE Journal 50, no. 12 (2004): 3034-3048.

[36]. Bryant, Steven L., Peter R. King, and David W. Mellor. "Network model evaluation of permeability and spatial correlation in a real random sphere packing." Transport in Porous Media 11, no. 1 (1993): 53-70.

[37]. Mellor, David W. "Random close packing (RCP) of equal spheres: structure and implications for use as a model porous medium." PhD diss., Open University, 1989.

[38]. Reboul, Nadège, Eric Vincens, and Bernard Cambou. "A statistical analysis of void size distribution in a simulated narrowly graded packing of spheres."Granular Matter 10, no. 6 (2008): 457-468.

[39]. Al-Raoush, Riyadh, Karsten Thompson, and Clinton S. Willson. "Comparison of network generation techniques for unconsolidated porous media." Soil Science Society of America Journal 67, no. 6 (2003): 1687-1700.

[40]. Balhoff, Matthew T., and Karsten E. Thompson. "Modeling the steady flow of yield- stress fluids in packed beds." AIChE Journal 50, no. 12 (2004): 3034-3048.

[41]. “Chi-square goodness-of-fit test” The MathWorks, Inc., accessed October 22, 2015, http://www.mathworks.com/help/stats/chi2gof.html.